



Crustal structure and magmato-tectonic processes in an active rift (Asal-Ghoubbet, Afar, East Africa): 1. Insights from a 5-month seismological experiment

C Doubre, I Manighetti, C Dorbath, L Dorbath, E Jacques, J. C. Delmond

► To cite this version:

C Doubre, I Manighetti, C Dorbath, L Dorbath, E Jacques, et al.. Crustal structure and magmato-tectonic processes in an active rift (Asal-Ghoubbet, Afar, East Africa): 1. Insights from a 5-month seismological experiment. Journal of Geophysical Research, 2007, pp.B05405. 10.1029/2005JB003940 . insu-01284899

HAL Id: insu-01284899

<https://hal-insu.archives-ouvertes.fr/insu-01284899>

Submitted on 8 Mar 2016

HAL is a multi-disciplinary open access archive for the deposit and dissemination of scientific research documents, whether they are published or not. The documents may come from teaching and research institutions in France or abroad, or from public or private research centers.

L'archive ouverte pluridisciplinaire **HAL**, est destinée au dépôt et à la diffusion de documents scientifiques de niveau recherche, publiés ou non, émanant des établissements d'enseignement et de recherche français ou étrangers, des laboratoires publics ou privés.

Crustal structure and magmato-tectonic processes in an active rift (Asal-Ghoubbet, Afar, East Africa):

1. Insights from a 5-month seismological experiment

C. Doubre,^{1,2,3} I. Manighetti,^{1,4} C. Dorbath,^{5,6} L. Dorbath,^{5,6} E. Jacques,^{1,7} and J. C. Delmond⁷

Received 13 July 2005; revised 25 July 2006; accepted 15 November 2006; published 10 May 2007.

[1] We seek to characterize how magmatic and tectonic activities combine and interact during the continental rifting process. We address this question in two companion papers. In both, we analyze the seismicity that occurs in an active magmato-tectonic rift, Asal-Ghoubbet (East Africa), to identify the features and/or processes responsible for its activity. Here, we report results from a 5-month experiment that we conducted in the rift. Eleven seismometers were deployed to complement the eight-station permanent network. This allowed recording ~400 earthquakes in the rift; 200 events could be well located (precision <40 m) and used in a tomographic inversion. Focal mechanisms were also determined for 71 events. The results show that current activity in the rift is mainly magmatically induced or accommodated. A ~2-km-wide pipe of hot rock is evidenced below the central Fieale-Shark Bay volcanic complex, likely above a deeper (>5–6 km) magma reservoir. Most events concentrate at the roof of the pipe (at 3–4 km) and result from up and down slip ruptures on both the volcanic (ring) and tectonic faults that enclose the pipe at depth. The up and down motions are likely driven by pressure changes in the magma reservoir. Hence, although a few rift faults were associated with seismicity, most remained seismically silent during the experiment. In the companion paper, we analyze the seismic activity in the rift over the 23 years that followed its last rifting episode. This confirms the importance of the Fieale-Shark Bay plumbing system in the overall rift behavior.

Citation: Doubre, C., I. Manighetti, C. Dorbath, L. Dorbath, E. Jacques, and J. C. Delmond (2007), Crustal structure and magmato-tectonic processes in an active rift (Asal-Ghoubbet, Afar, East Africa): 1. Insights from a 5-month seismological experiment, *J. Geophys. Res.*, 112, B05405, doi:10.1029/2005JB003940.

1. Introduction

[2] About two thirds of the Earth's crust is created by spreading at mid-ocean ridges. Yet the detailed nature of the plate accretion process is still partially unknown [e.g., Barclay *et al.*, 1998; Crawford *et al.*, 1999; Escartin *et al.*, 1999; Hussenoder *et al.*, 2002]. Among other questions, one is to understand how magmatic and tectonic activities combine and interact to thin, break, and split apart a lithospheric plate. We here regard that question at the very

first stage of the spreading process, which is the stage of continental rifting. That initial stage of rifting, through which a continental plate evolves from stretching to breaking, is of particular importance for it may govern the way subsequent oceanic spreading will occur. Yet, little is known on that rifting process, for rare are the places in the world where it currently occurs; generally, rifting has either come to an end and been replaced by oceanic spreading, or has aborted before a new ocean could be formed. In both cases, the initial rift structures are “frozen”, i.e., not active anymore, so that their analysis, even detailed, cannot allow the rifting process to be fully documented.

[3] We here focus on the only place in the world, East Africa, where continental, magmato-tectonic rifting is currently going on and accessible to direct observation. Indeed, although two young oceans (Red Sea and Gulf of Aden) separate Arabia from Africa, the breaking of the two continental plates is not yet complete; the two plates are still “attached” in the Afar region [e.g., Varet, 1978; Courtillot, 1982; Manighetti *et al.*, 1997]. As a consequence, the Afar depression is the site of active rifting that mainly takes place along a series of disconnected rift segments [e.g., Varet, 1978; Tapponnier *et al.*, 1990; Manighetti

¹Laboratoire de Tectonique, Institut de Physique du Globe de Paris, Paris, France.

²Laboratoire de Géodynamique des Rifts et des Marges Passives, Université du Maine, Le Mans, France.

³Now at Department of Earth and Space Sciences, University of California, Los Angeles, California, USA.

⁴Now at Laboratoire de Géophysique Interne et Tectonophysique, Grenoble, France.

⁵Ecole et Observatoire des Sciences de la Terre, Strasbourg, France.

⁶Institut de Recherche pour le Développement, Paris, France.

⁷Volcanologic Observatories, Institut de Physique du Globe de Paris, Paris, France.

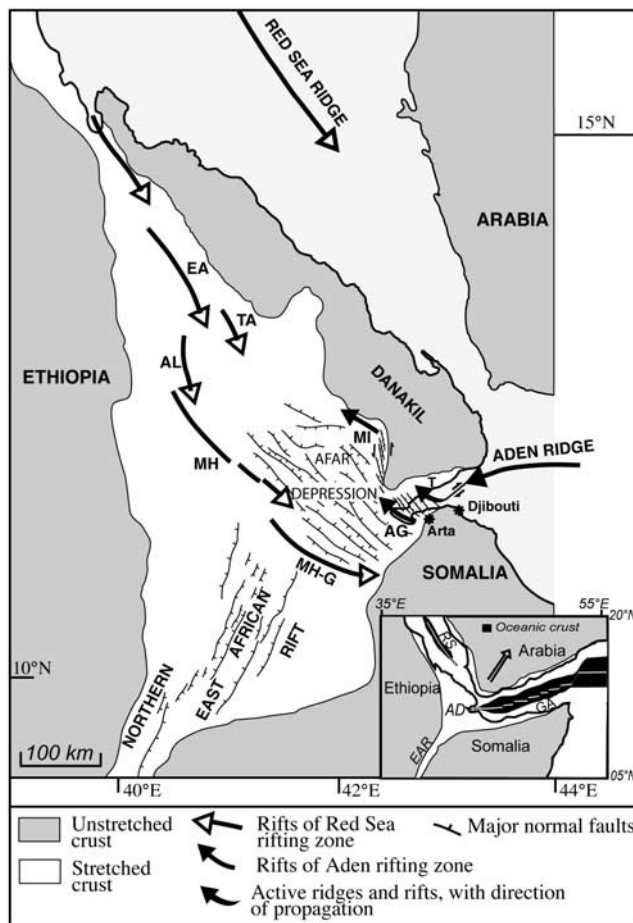


Figure 1. Simplified structural map of Afar Depression (redrawn from *Manighetti et al.* [1997, 2001b]). Rift segments in capital letters, with MI, Manda Inakir; AG, Asal-Ghoubbet; T, Tadjoura; EA, Erta Ale; TA, Tat'Ali; AL, Alayta; MH, Manda Hararo; MH-G, Manda Hararo-Goba'ad. Inset shows general plate tectonic context. EAR, East African Rift; RS, Red Sea ridge; GA, Gulf of Aden ridge; AD, Afar Depression. Arrow indicates Arabia-Africa divergent plate motion.

et al., 2001b] (Figure 1). These segments are all sites of localized active faulting and volcanism. Among them, one, Asal-Ghoubbet (AG), is easily accessible to field observation [e.g., *Needham et al.*, 1976; *Abdallah et al.*, 1979; *Stieljes*, 1980; *Stein et al.*, 1991; *Manighetti et al.*, 1998]. We thus focus on that rift, and seek to characterize how magmatic and tectonic activities combine and interact to make the rift stretch apart (rate of 16 ± 1 mm/yr [e.g., *Vigny et al.*, 2007]). We address this question at the current timescale. Our approach is to analyze the seismicity that occurs in the rift, and seeks how it relates to the ongoing magmato-tectonic processes. Such an approach is made possible because a permanent seismological observatory (Centre de Recherche Scientifique de Djibouti (CERD) and Institut de Physique du Globe de Paris, France) exists in the rift that has been continuously recording its seismic activity over the last 30 years. Because the rift extends on dry land, temporary seismological experiments can also be conducted and provide even more accurate data. The Asal-

Ghoubbet Rift thus is a unique field laboratory where seismological investigations can be performed at the greatest level of detail.

[4] We analyze current seismicity in AG at two different timescales, which we describe in two papers.

[5] The present paper is a detailed analysis of the micro-seismicity recorded during a 5-month experiment that we conducted in the rift during the winter 2000–2001. A total of 208 microearthquakes were precisely located, 200 of them in the central emerged part of the rift. We thoroughly analyze these earthquakes to answer the following questions: How is current seismic activity distributed in the rift? What are the structures and/or processes responsible for that activity? What is the crustal structure of the rift, and how is that structure related to tectonic and magmatic features? The spatial coverage and the number of events allow us to perform a three-dimensional (3-D) inversion and derive the crustal structure of the central part of the rift down to 5 km depth. The seismic events are simultaneously located with uncertainties of a few tens of meters. The well-constrained event distribution reveals that only a few zones were sites of seismicity in the 5 months of recording, with the Fieale caldera being the most active zone. The determination of 71 focal solutions sheds light on the mechanisms responsible for the recorded events. Together these results allow us to discuss both the rift structure, and the way tectonic and magmatic processes may be currently interacting. Note that our data are the first to be acquired in the AG Rift at such level of accuracy. They also are the first to provide insights on the magmatic plumbing and 3-D architecture of the rift.

[6] *Dobre et al.* [2007] present the analysis of the entire set of available earthquake data that have been recorded in the rift by the permanent observatory since the last 1978 rifting episode (period 1979–2001; ~ 2500 events down to a magnitude of -1.0). Such a long and continuous recording allows the overall space-time evolution of seismicity to be depicted, the crustal structure to be refined, and the mechanisms possibly responsible for the rift seismicity to be further discussed. Together the results highlight how the rift has behaved overall since its last opening episode, and kept opening through ongoing magmato-tectonic interactions. Combined with previous results obtained on other rift/ridge segments worldwide, the work brings new insights to further understand the rifting process.

[7] Note that while complementary, the two papers can be read independently. Yet, the conceptual scenario that we envision as best describing the current behavior of the rift is only described in the second paper, where it is constrained by all available data.

2. Geological Setting

[8] Rifting in Afar is going on since ~ 20 Ma as a result of Arabia moving away from Africa [e.g., *Courtillot et al.*, 1980, 1987; *Tapponnier et al.*, 1990; *Manighetti et al.*, 2001b]. It mainly occurs along a series of disconnected, NW striking, 20- to 40-km-long volcano-tectonic rift segments that extend on either sides of the Afar depression (Figure 1) [*Tapponnier et al.*, 1990; *Hayward and Ebinger*, 1996; *Manighetti et al.*, 1997, 1998, 2001b]. These rift

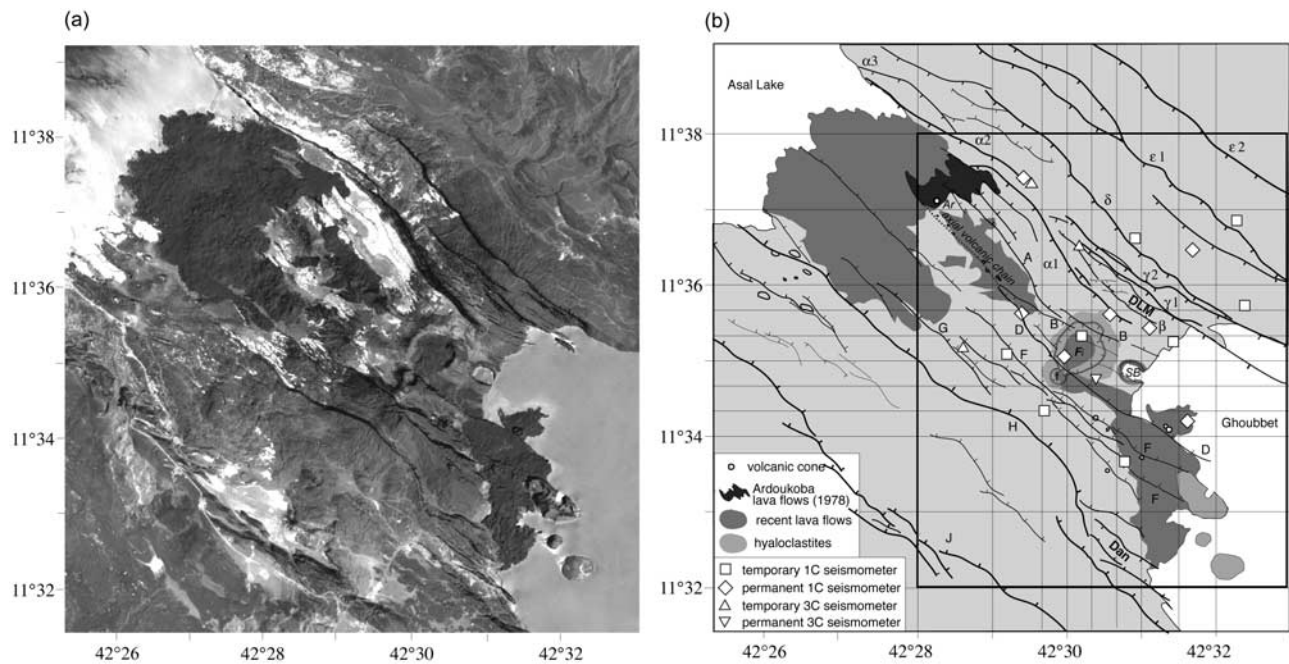


Figure 2. (a) Satellite SPOT image of subaerial section of Asal-Ghoubbet Rift combined to DEM [from *De Chabaliér and Avouac*, 1994], showing major tectonic and volcanic features between Asal lake and Ghoubbet. (b) Interpretation of Figure 2a, showing major faults (from *Manighetti et al.* [2001a]; named by letters) and volcanic features (Fi, SB, and F for Fieale, Shark Bay, and F calderas; Ar for Ardoukoba volcano). DLM and Dan for Disa Le Mallo and Dankalelo subrifts, respectively [from *Manighetti et al.*, 1998]. Permanent and temporary networks are shown. Grid is that used for tomographic inversion.

segments have different ages and degrees of evolution, for the whole rifting process was diachronic.

[9] Asal-Ghoubbet is one of the youngest rifts, with an age of ~ 0.9 Ma [Varet, 1978; Courtillot *et al.*, 1980; Manighetti *et al.*, 1998]. As any other rifts in Afar, AG is a narrow zone (~ 15 km) of localized active faulting and magmatism. It currently opens at 16 ± 1 mm/yr in a $N40 \pm 5^\circ E$ direction [e.g., Ruegg and Kasser, 1987; Vigny *et al.*, 2007] (Figures 1–3). Although a bulk of studies have been conducted in the AG Rift in the last 30 years [e.g., Needham *et al.*, 1976; Abdallah *et al.*, 1979; Stieljes, 1980; Stein *et al.*, 1991; De Chabaliér and Avouac, 1994; Manighetti *et al.*, 1998, 2001a, 2001b; Audin *et al.*, 2001; Mlynarski and Zlotnicki, 2001; Ballu *et al.*, 2003], its 3-D architecture is unknown, as are the precise respective contributions of faulting and magmatism in its opening. The only clear finding is that magmatic and tectonic activities have been combining over the whole rift evolution; phases of dominant magmatic activity have alternated with phases of major faulting [Stein *et al.*, 1991; De Chabaliér and Avouac, 1994; Manighetti *et al.*, 1998]. During the former, large volumes of fissural basaltic lavas have filled the rift inner floor, burying existing faults. During the latter, faulting have dismantled the lava pile. That scenario particularly applies for the last ~ 300 ka. Between ~ 300 and 100 ka, thick volcanic series were emplaced in the rift inner floor (bounded at that time by faults J and ϵ ; see Manighetti *et al.* [1998] for details), most from the central Fieale shield volcano (Fi, Figure 2) supposedly fed by a long-lived, deep magma chamber [Van Ngoc *et al.*, 1981]. These lava flows progressively buried most previous faults. Magmatic activity then almost completely ceased at ~ 100 ka. Faulting thus

resumed and progressively dismantled the lava pile, only interrupted from time to time by short phases of fissural volcanism (such as those responsible for the recent lava fields that extend on either sides of the Fieale edifice, Figure 2). The normal fault scarps that are presently observed to shape the AG Rift were formed during that “amagmatic,” a ~ 100 -ka-long period.

[10] One may thus conclude that since 100 ka, faulting is the process most contributing to the rift opening [Stein *et al.*, 1991]. The rift normal faults indeed form impressive, steep (70 – 80°) escarpments at surface, some as high as 200 m. The faults form a dense network that deeply shapes the rift from the western shore of the Asal Lake to the west, to the easternmost part of the Ghoubbet basin to the east (over ~ 40 km long; Figure 3). Hence, while only the 15-km-long western section of the rift is emerged, faults extend further east in the Ghoubbet (Figures 2 and 3). The analyses that have been performed on the rift faults reveal that most, including those in Ghoubbet, have been active in recent times (<10 – 20 ka), and slipping at fast rates (several mm/yr up to present [Ruegg and Kasser, 1987; Ruegg *et al.*, 1990; Stein *et al.*, 1991; Manighetti *et al.*, 1998; Audin *et al.*, 2001; Doubre *et al.*, 2005; Vigny *et al.*, 2007]). Fault activity also has migrated northward with time, so that the northernmost faults (from α to δ), particularly those forming the “Disa Le Mallo subrift” (DLM; Figure 2), are the youngest and most active at present [Manighetti *et al.*, 1998].

[11] The AG Rift thus is clearly the site of recent and likely current tectonic activity. Yet, the rifting episode that stroke the rift in November 1978 was essentially magmatic; the sudden ~ 2 -m opening of the rift apparently resulted

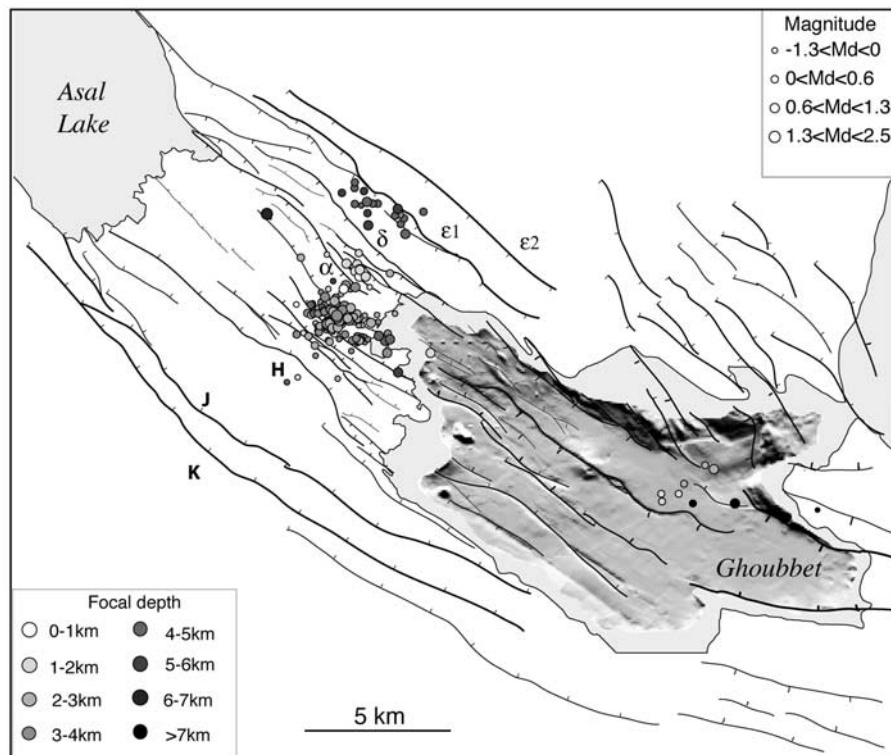


Figure 3. Initial localizations of recorded events, superimposed on rift fault map. The western half of the rift is above sea level while the Ghoubbet basin is submerged. Bathymetry from Audin *et al.* [2001]; faults from Manighetti *et al.* [1998, 2001a, 2001b] and Audin *et al.* [2001].

from the injection of two major magmatic dikes at depth [Ruegg *et al.*, 1979; Tarantola *et al.*, 1979, 1980]. While the event was accompanied with two moderate earthquakes ($m_b = 5$ and 5.3) and slip on a few rift faults (in inner floor and northern rift shoulder [Abdallah *et al.*, 1979; Le Dain *et al.*, 1979; Lépine *et al.*, 1980]), its major “component” was a week-long basaltic fissural eruption at the northwestern tip of the axial volcanic chain (Figure 2) that gave birth to the so-called Ardoukoba volcano [e.g., Demange *et al.*, 1980]. The 1978 episode thus demonstrates that the AG Rift also is the site of current magmatic activity. The numerous recent lava flows that pave the rift inner floor suggest that similar volcanic activity has occurred in the recent past.

[12] Our objective is to bring data that may help further documenting the magmato-tectonic and possibly other processes that are currently operating in the rift. We also seek to bring constraints on the 3-D structure of the rift, for it is unknown at present, even at first order. We follow a seismological approach (passive recording), and use it as a tool to illuminate the major “sources” of current activity and infer their distribution, nature and behavior.

3. Data Acquisition and Processing

3.1. Temporary Seismic Network

[13] At the end of 2000 we deployed a seismic network of 11 stations in the central part of the Asal-Ghoubbet Rift where greater seismic activity was expected [e.g., Lépine and Hirn, 1992] (Figure 2b). The network was operated for 5 months from 20 October to 22 March 2001, complementing the 15 stations of the permanent network operated by

the Arta Geophysical Observatory (eight stations in the rift (Figure 2b), one on the Ghoubbet shore, four on either sides of the Gulf of Tadjoura, and two in the center of the Djibouti territory (not represented)). The temporary network included eight telemetered stations (Mark Product L4C, vertical sensor) and three autonomous 3-C stations (GEOSTAR, 150 Hz sampling, continuous recording, MarkProduct L22 and L4 3 component sensors), all belonging to Ecole et Observatoire des Sciences de la Terre of Strasbourg, France. The stations were deployed on a $8 \times 8 \text{ km}^2$ area encompassing the Fieale caldera, the Ghoubbet western coast, the DLM subrift and the eastern half of the northern rift shoulder (Figure 2b). Their mean spacing was chosen to be less than the expected mean hypocentral depth (according to Bulletins of Arta Geophysical Observatory), hence $< 2 \text{ km}$. The autonomous stations were fitted with GPS receivers. The digital signals of the telemetered stations were transmitted by FM radio waves and recorded continuously at the Arta Geophysical Observatory ($\sim 35 \text{ km}$, Figure 1).

3.2. First Hypocenter Localizations

[14] More than 600 events were recorded, most of them were local, i.e., occurring within the AG Rift. Our focus is on these local events.

[15] The P and S wave arrival times were picked by hand from numerical records (precision of 0.01 s). The S wave arrivals were less numerous, and their arrival times less accurate when read on 1C stations (only three 3C stations allowing high-precision picking). We used the program Hypoinverse [Klein, 1978] to determine the preliminary hypocentral location of the best recorded events, i.e.,

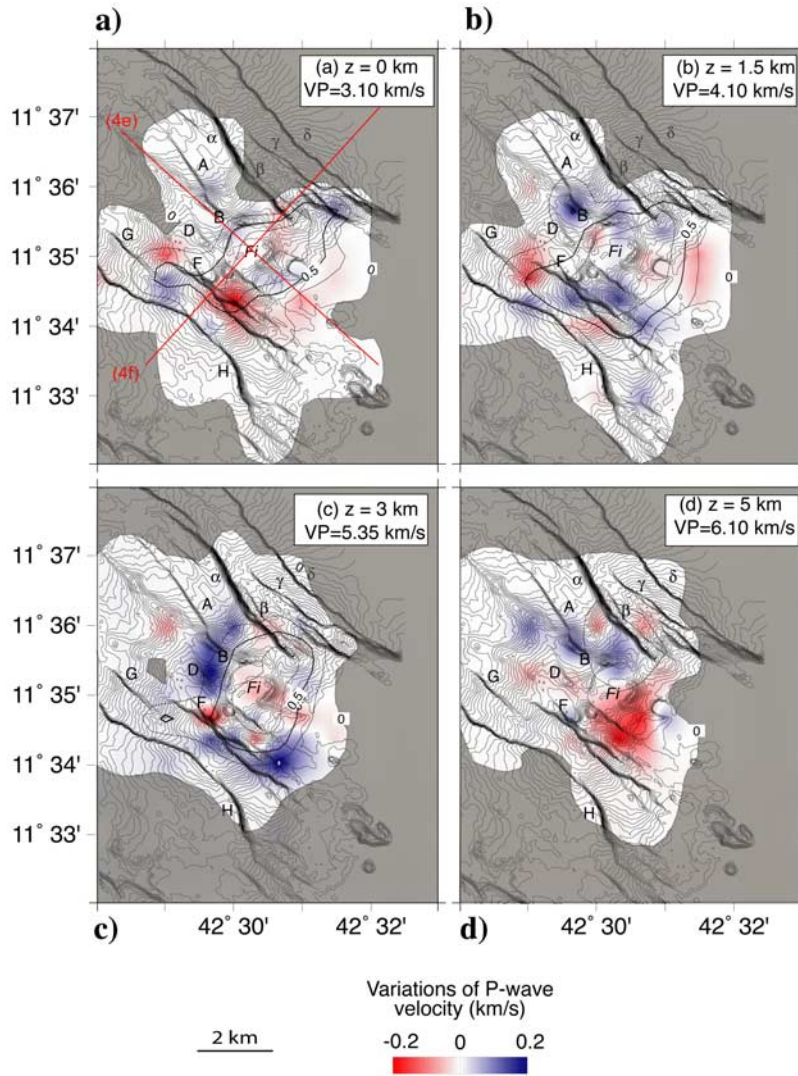


Figure 4. P wave velocity variations at (a) 0, (b) 1.5, (c) 3 and (d) 5 km depth, and on (e) rift-parallel and (f) rift-perpendicular cross sections intersecting at Fieale (location in Figure 4a). Resolution isocurves are shown. Unresolved zones are shaded. In Figures 4a–4d, the value of V_p from initial 1-D model is indicated. Fi for Fieale caldera. In Figures 4e and 4f, velocities are linearly interpolated between depths of calculation. Curves of no velocity change are dotted. Main faults and volcanic features are shown on corresponding topographic sections.

events for which P and S waves had been recorded and identified at a minimum of 8 and 1 stations, respectively. This resulted in running calculation on 430 events. We used a one-dimensional crustal velocity model previously derived from a seismic refraction experiment conducted in the same area [Ruegg, 1975]. The model suggests a variation of V_p with depth that is comparable overall to that inferred from similar volcano-tectonic environments (auxiliary material Figure S1 and references therein).¹

[16] Using Hypoinverse, we explored the depth range 1–9 km expected to be the maximum thickness of the brittle crust in AG Rift [Ruegg, 1975]. Only 301 events satisfied the following criteria: $RMS \leq 0.25$ s, horizontal (erh) and vertical (erz) errors ≤ 1.5 km, and conditioning factor ≤ 50 .

Among them, 208 events were found in the AG Rift, all within the entire network (temporary + permanent). They have a mean erh, erz, and RMS of 410 m, 510 m and 0.06 s, respectively. These events are plotted on the structural map of the rift in Figure 3. Most of them (200) are distributed in the central, subaerial part of the rift, all within the temporary network, while eight of them are in the Ghoubbet. All range between 0 and 7.7 km depth. The magnitudes have been calculated with a formula established in the somehow similar Yellowstone volcano-tectonic environment: $M_d = -2.60 + 2.44 \log D$, with D the signal duration [Pechmann et al., 2001]. They do not exceed 2.5, with a mean of 0.5.

3.3. Tomographic Inversion

[17] The number and spatial distribution of the events recorded within the temporary network (200 events) make them well suited for tomographic inversion. The purpose of

¹Auxiliary materials are available in the HTML. doi:10.1029/2005JB003940.

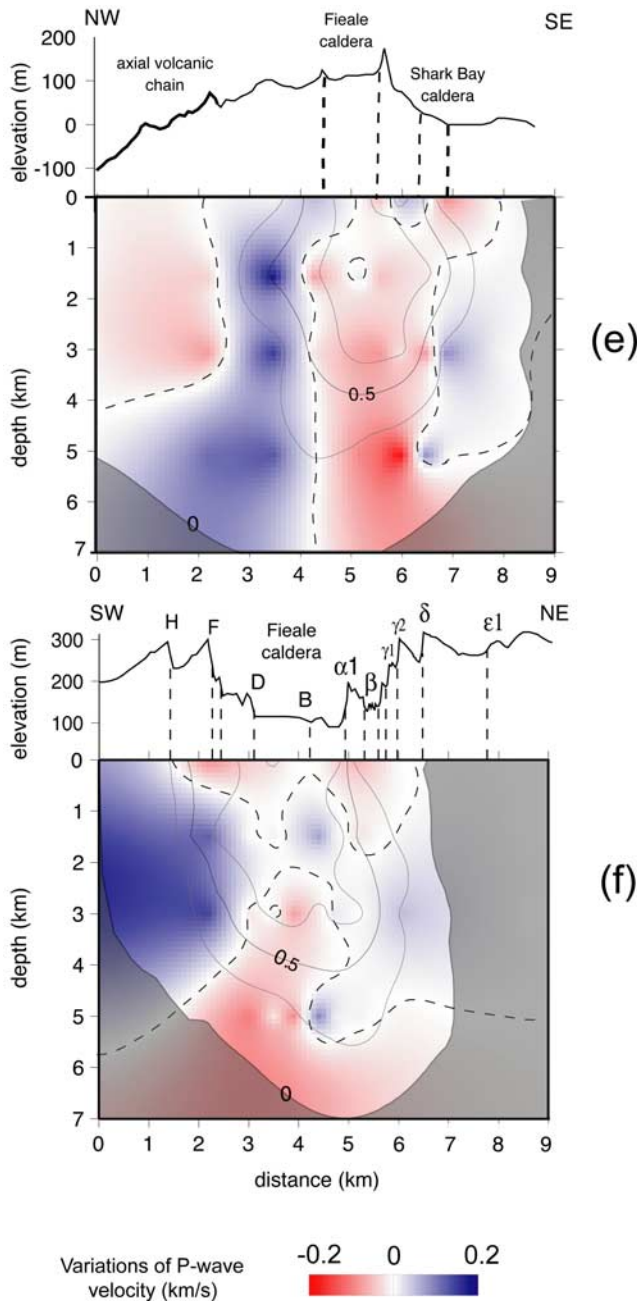


Figure 4. (continued)

such an inversion is to simultaneously determine the three-dimensional crustal velocity model and refine the event hypocentral parameters.

[18] We performed the inversion using the software Simulps12 [Evans *et al.*, 1994] that is based on a method developed by Thurber [1983] and subsequently improved by Eberhart-Phillips [1990]. As shown by Arnott and Foulger [1994a; see also Thurber, 1984; Eberhart-Phillips, 1986; Toomey and Foulger, 1989], such a method is well adapted to volcano-tectonic environments such as those in Iceland, Hawaii or Afar.

[19] The square in Figure 2b shows the area where we performed the inversion. The volume studied is viewed as a 3-D grid of $11 \times 7.5 \times 5 \text{ km}^3$, with a tighter nodal spacing, 0.6 km, in its central part where earthquake density is greater (Figures 2b and 3). The depth distribution of events (0–7.7 km) limits us to perform the inversion at four depth levels only (0, 1.5, 3 and 5 km). The initial three-dimensional velocity model is deduced from the 1-D model of Ruegg [1975]. Starting with this initial model, Simulps12 runs successive, iterative inversions, until the most refined three-dimensional crustal structure and hypocentral parameters are obtained. Note that all stations being inside the grid, we ran the inversions without station correction.

[20] A total of 2143 P wave and 1798 S wave arrival times were inverted. A suite of damping values was tested. That of $20 \text{ s}^2/\text{km}$ revealed to be the best compromise between data misfit and model variance. The small RMS (0.06 s on average) of the Hypoinverse solutions for the 200 earthquakes within the grid allowed the calculations to be achieved after five iterations only, the model and data variance being then reduced by 39 and 32%, respectively. Figure S2 shows the resolution at the four depth levels. Reliable solutions are obtained in the top 3 km where most events occurred (Figures S2a–2c). At greater depth where rays were fewer and mainly coming from the north, the solutions are less constrained (Figure 2d).

[21] The P and S wave velocities slightly changed (by <0.2 and $<0.07 \text{ km/s}$, respectively) during the inversion. The largest variations are found for the P waves (Figure 4) and are the only ones retained for discussion in section 3.4. Indeed, because of lower resolution, S wave velocity changes are small and not larger than uncertainties. We thus consider that these changes are not meaningful. The V_p/V_s calculations performed by Simulps12 therefore are not either.

[22] A number of tests were conducted on our final model of P wave velocity anomalies (Figure 4), in order to test for its strength. Different grid rotations were performed to check whether or not aligning the grid nodes parallel or perpendicular to the rift would distort the anomalies depicted in Figure 4. We found that they were not distorted. We thus present the final model in its most readable form, i.e., with no rotation. We also ran a forward model (i.e., in which earthquake location is taken as known) to test for possible smearing and check how recoverable the anomalies identified in Figure 4 were with the raypaths. That forward model is shown in Figure S3. It basically confirms that though they have smaller amplitudes as expected from the forward calculation, the major anomalies visible in Figure 4 are still found, with the same overall distribution. Together these comfort us that the major features of Figure 4 are well constrained. The low-amplitude P velocity changes suggest that the initial 1-D velocity model [Ruegg, 1975] is appropriate overall. Yet the refined velocities are slightly faster, so that the V_p -depth curve further resembles those inferred in Iceland, Mid-Atlantic Ridge, and East Pacific Ridge (Figure S1).

3.4. Hypocenter Relocations

[23] Final hypocentral locations lay in the range 0–7.14 km, with horizontal and vertical errors of $\sim 40 \text{ m}$ (Figure 5). While relocated hypocenters show an overall

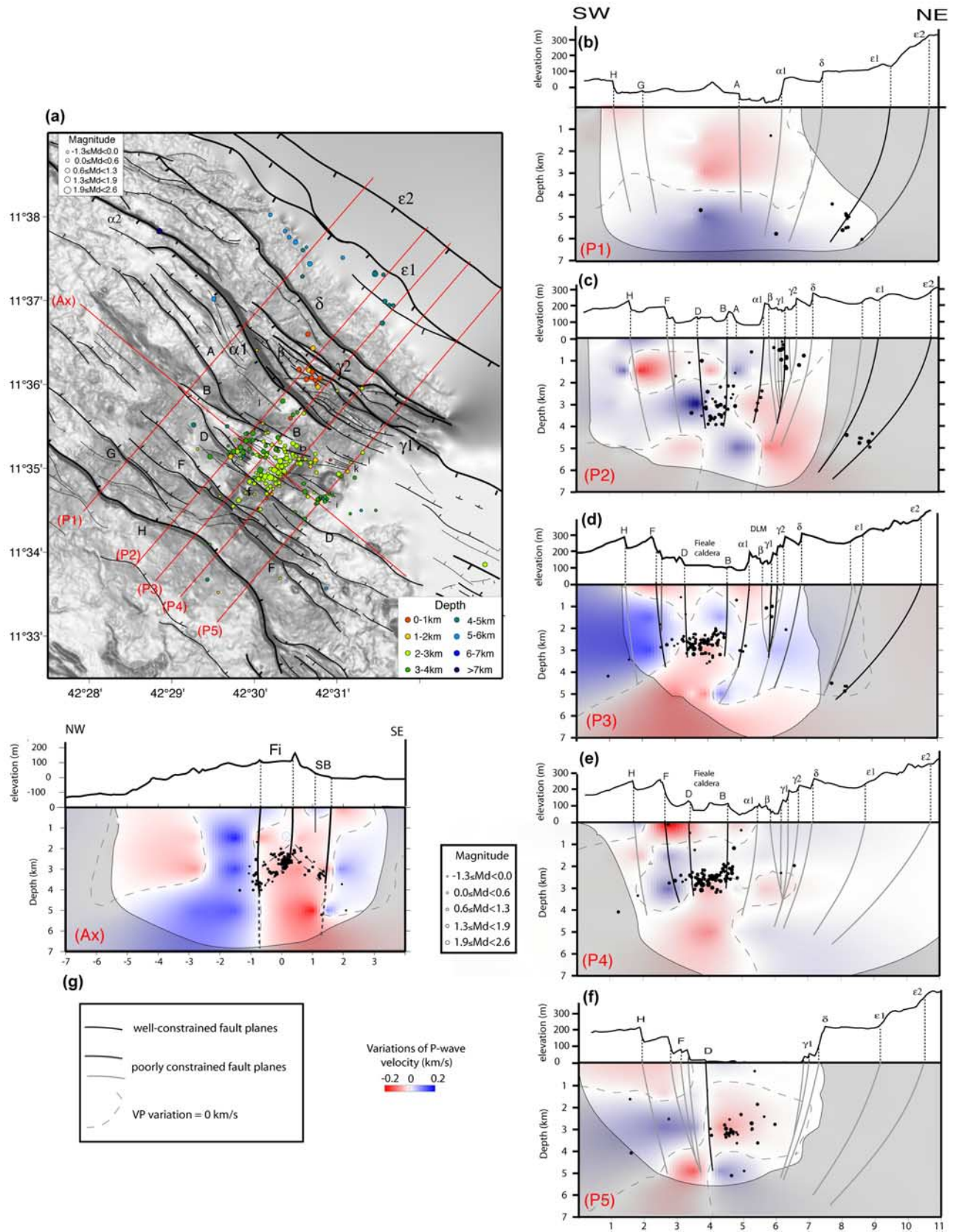


Figure 5. Relocated events (a) in map and (b–g) on cross sections (location in Figure 5a). Tomographic results are shown on the cross sections with unresolved zones in gray. Fi and SB, Fieale and Shark Bay calderas, respectively.

shallowing (by ~ 170 m on average) compared to their previous Hypoinverse position, they do not show any systematic lateral offset (compare Figures 3 and 5a). The distance between the initial and relocated positions of 95% of the earthquakes varies from 0 to 1.46 km, with a mean of 420 m. The remaining 10 events' hypocenters moved more than 1.5 km after relocation. We suspect that such events had poorly constrained Hypoinverse hypocenters, stuck close to one interface of the layered 1-D crustal model.

[24] The clusters of relocated events are narrower normal to the major NW striking faults (see for instance ε system), and many relocated events clearly move toward fault planes (see for instance α fault). This results in narrow clusters of events being aligned parallel to the major faults, with their epicenters in the hanging wall of these faults (see $\varepsilon 1$, $\gamma 1$, $\alpha 1$, D). Within the Fieale caldera, most relocated events move out toward the caldera edges (see eastern edge). Taken together these observations further confirm that the 3-D crustal model is robust.

3.5. Focal Mechanisms

[25] We constructed focal mechanisms for 71 events, by mapping the distribution of P wave first motion polarities on the lower focal hemisphere. We used the ray azimuths and takeoff angles obtained when using the 3-D crustal model. All focal planes were hand mapped, for the large number of phases (≥ 8 in all cases) ensured their precise determination. The 71 focal solutions are shown in Figure S4, together with the polarities. The latter are shown in more details for four example events in Figure S5. Assuming that most earthquakes correspond to shearing on a fault plane, double-couple solutions were preferred when possible. We determined 55 double-couple mechanisms (DC, Figure 6, Figures S4 and S5, top plots). About 70% of them attest to normal faulting on steep planes (dip $75 \pm 10^\circ$ when the steepest focal planes are chosen) striking $N120 \pm 20^\circ E$ or $N0 \pm 20^\circ E$. About 40% of these normal mechanisms indicate pure or mainly dip-slip motion, while the others reveal an additional component of lateral slip. The remaining $\sim 30\%$ of the double-couple solutions attest to strike-slip ($\sim 13\%$) and even reverse faulting, on planes with various dips and strikes nearby a direction orthogonal to the rift axis.

[26] Although their polarities were determined with certainty (see Figure S5, bottom plots), 16 events were inconsistent with a double-couple solution (Figure 6 and Figure S4). One of these events shows compressional arrivals only, another one dilatational arrivals only, and 14 events a mixture of the two. A detailed seismological analysis of these specific events is beyond the scope of this paper. We thus solely report their main features. In most cases the nondouble-couple mechanisms (NDC) show polarities separated by two roughly parallel planes. Similar NDC mechanisms have already been found in the AG Rift, mainly in the Fieale area [Lépine and Hirn, 1992]. Such mechanisms are also quite common in volcanic regions [e.g., Foulger and Long, 1984; Foulger, 1988a, 1988b]. Mechanisms showing only compressional or dilatational polarities are commonly taken to attest to explosions or cavity collapses, respectively [e.g., Foulger et al., 1989], or to the nucleation/opening of tensional fractures having a strike-slip component [Aki, 1984; Shimizu et al., 1987]. Mechanisms showing a combination of compressional and

dilatational polarities are more likely taken to attest to a variability of the elastic moduli within the source volume [e.g., Julian et al., 1988], or to tensional fracturing/fissuring such as that resulting from thermal contraction or expansion of the rocks or from hydraulic/hydrothermal processes [e.g., Foulger and Long, 1984; Julian, 1983; Aki, 1984; Foulger et al., 2004]. In the latter cases, the mechanisms show polarities separated by two roughly parallel planes that define the plane of fissuring. Frohlich [1984] suggests that such a distribution of polarities may also be induced by simultaneous slip on various planes, as those typifying circular ring-type or cone-shaped faults [Ekström, 1994; Nettles and Ekström, 1998].

4. Data Analysis

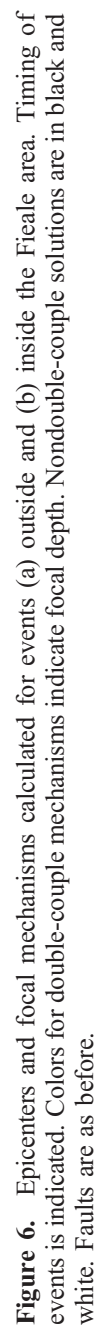
4.1. Velocity Anomalies

[27] The tomographic inversion only allows depicting the crustal structure in the eastern emerged part of the rift. We focus on the areas crossed by many rays and thus best constrained: Fieale, northern subrift and western Ghoubbet coast.

[28] Figure 4 presents the variations of the P wave velocities at the four depth levels of the inversion (Figures 4a–4d), and on two cross-sections, parallel (Figure 4e) and perpendicular (Figure 4f) to the rift and intersecting in the Fieale caldera (location in Figure 4a). On both cross sections the velocity variations have been linearly interpolated between the nodes.

[29] The P wave velocity slightly changes laterally at all depth levels (≤ 0.2 km/s). In similar volcano-tectonic environments, P wave contrasts are found to be much higher, between 0.7 and 1.4 km/s in the Mid-Atlantic Ridge [Wolfe et al., 1995; Barclay et al., 1998; Madge et al., 2000], and possibly up to 2 km/s in the Krafla Icelandic volcano [Arnott and Foulger, 1994a]. Although small, the largest velocity anomalies define a few clear, well-constrained major volumes (see section 3.3), which we describe below.

[30] Contrary to what is commonly observed in oceanic ridge segments [e.g., Toomey et al., 1990; Wilcock et al., 1995], the zones of velocity anomalies do not show any clear symmetric pattern with respect to the rift axis, nor are they shaped or aligned parallel to the rift axis. Rather their distribution draws a circular pattern roughly centered at the Fieale caldera (Figures 4 and S3). This is particularly clear at the 3 km depth level (Figure 4c) and on the cross sections (Figures 4e and 4f). A well-resolved, ~ 1.5 -km-wide, almost continuous ring of positive (blue) anomaly surrounds the zone that extends directly at 3 km below the Fieale caldera. On both cross sections, that ring of positive anomaly seems to extend further upward and downward, so that the whole volume looks rather like a cylinder of positive anomaly surrounding the “Fieale zone”. That zone is the site of a large negative (red) anomaly that appears as a vertical, ~ 2 -km-wide, central column rising from 5 km depth and possibly more, up to 2–1 km, within the “blue cylinder” (Figures 4e and 4f). The maximum velocity contrast within this column is found at 5 km depth, at the southeastern edge of the Fieale caldera (Figure 4d). Although not strongly constrained (Figure S2), that contrast is well recovered in the forward test (Figure S3), suggesting that it is real. In Figure 4e, the boundaries between the blue and red anomaly



zones appear as sharp and subvertical discontinuities, particularly to the west. The western boundary extends right below the western edge of the present Fieale caldera, while the eastern boundary lies below the eastern edge of the small Shark Bay caldera that is adjacent (and likely connected at depth) to that of Fieale.

[31] Despite of the low resolution, the volcanic chain that extends west of Fieale appears underlined by a wide negative anomaly that extends from surface down to ~ 3 km (Figure 4e). The amplitude of that anomaly is, however, too low for that anomaly to be recovered in the forward test presented in Figure S3.

[32] Velocity changes found at or close to the surface are more disorganized. The shallow levels seem dominated overall by high-velocity material (Figures 4a, 4b, 4e, 4f, and S3). Yet a few small patches of negative anomaly are identified, most either at the tip of some major faults (see eastern tip of fault α), or in the relay zones between faults (see area between faults G and F, and central section of fault system F where several fault segments intersect). A patch of negative anomaly is also found below the Shark Bay caldera.

[33] The possible origin of the velocity contrasts described above will be examined in the discussion section.

4.2. Earthquake Distribution and Kinematic Behavior of Main Seismic Zones

[34] Figure 5a plots the epicenters of the 200 relocated earthquakes on top of a digital elevation model of the AG Rift where major structures can be seen.

[35] The combination of Figures 3 and 5 shows that although most faults in the rift show evidence of recent activity (<10 – 20 ka; see section 2), little seismicity is observed, with most faults showing no earthquake at all on or close to their surface trace. Similarly, although several recent hence active volcanic zones exist in the rift, including the 1978 Ardoukoba, only the Fieale/Shark Bay volcanic area is underlined by seismicity. Besides, events are unevenly distributed in the rift, with most of them concentrated in the central, northeastern part of its subaerial section. Observed in more detail, these events appear to gather in three major distinct groups, one in the rift inner floor (Fieale area broad sense, between surface traces of F and B faults), one in the Disa Le Mallo subrift (between surface traces of β and δ faults), and one at the base of the northernmost ε fault system (Figure 5a). Events have homogeneous hypocentral depths in each group, averaging 2.9 km for the Fieale set, 1.1 km for the DLM set, and 5.1 km for the northern set. Only $\sim 8.5\%$ of the events spread outside of these clusters, being mostly along the α fault trace and in the southern rift shoulder.

[36] We describe each group in more detail below (on Figure 5 basis). The spatial distribution and focal mechanisms of events are used as a guide to identify the major structures (faults and volcanic features) possibly responsible for these events. Although we are aware that microruptures may have various origins and may not necessarily result from slip on major planar structures, their distribution delineates “rupture volumes” whose location, geometry and rupture mode may reveal and help characterize deformation on or associated with major structures. Note that the

present analysis will be refined in next section using the temporal evolution of the events.

4.2.1. Northern Rift Shoulder (North of δ Surface Trace)

[37] Sixteen events ($-0.9 \leq M_d \leq 1.3$) occurred in the northern rift shoulder, with their epicenters between the δ and $\varepsilon 1$ surface fault traces.

[38] The westernmost events are aligned parallel to the $\varepsilon 1$ trace, at a depth of 5–6 km. Projected on a plane perpendicular to the mean strike of $\varepsilon 1$ system, they fall on a plausible extension at depth of the fault plane (Figure 5b). This suggests that these events may result from slip on $\varepsilon 1$ plane, or from small-scale deformation associated with, but occurring off that plane (such as microcracking at fault plane edges or in the volume embedding the plane [e.g., *Manighetti et al.*, 2004, 2005]). In both cases, this would make $\varepsilon 1$ dipping to the SW by 60 – 75° at 5–6 km depth. Similarly relating the easternmost events to slip on or around $\varepsilon 1$ would make the latter having a subvertical plane in the east (Figure 5c). Since a fault is unlikely to sustain a 20 – 30° change in dip over such a short distance, we suspect that the easternmost events rather attest to slip on, or to secondary deformation around, the neighboring $\varepsilon 2$ fault plane. This would make $\varepsilon 2$ dipping south by 50 – 70° at ~ 5 km depth.

[39] The recorded events therefore show that micro ruptures occur on or around the northernmost ε fault system despite the lack of other evidence of its current activity (that system is among the oldest in the rift and does not show any morphological evidence of recent activity [*Manighetti et al.*, 1998]). The focal mechanisms determined for two of these events are nondouble couples, hence compatible with microcracking around the main fault planes.

4.2.2. Disa Le Mallo Northern Subrift

[40] The DLM subrift is taken to be the present locus of greatest tectonic activity in the rift [*Manighetti et al.*, 1998]. Its overall structure is that of a NW trending narrow graben bounded by antithetic normal faults (major are β , $\gamma 1$, $\gamma 2$, δ). The floor of the graben is dissected by a dense network of open fissures, some strike oblique (approximately E–W) to the faults.

[41] Sixteen events were located in the DLM subrift ($-0.5 \leq M_d \leq 1.0$), all concentrated in a $\sim 1 \times 1.5$ km² area in the center of the graben. All these events but two are extremely superficial, between 0 and 1.8 km depth. Most are vertically aligned below the most intensely fissuring zone, suggesting that they result from current fissuring and/or shallow slip on $\gamma 1$ (Figures 5c and 5d). Focal mechanisms rather support the fissuring origin. Four of the 11 calculated mechanisms are nondouble couple and likely result from NW–SE tensile cracking and explosion/implosions (Figure 6a). Five of the seven double-couple mechanisms attest to reverse faulting on $N40 \pm 20^\circ$ E striking planes. Taken together, these nine mechanisms are compatible with crack opening or closing in a local stress regime where σ_3 strikes \sim NE, as is the case in the rift. The two last mechanisms indicate normal slip on a steep, $\sim N130^\circ$ striking plane parallel to the faults, and strike-slip on oblique planes with one roughly parallel to the largest fissures in the zone.

4.2.3. Alpha Fault System

[42] The α fault system bounds the rift inner floor to the north over ~ 8 km long. It is one of the major systems in the

rift, being made of 3 en échelon, up to 200 m high, steep ($\sim 80^\circ$) fault escarpments facing to the south ($\alpha 1$, $\alpha 2$, $\alpha 3$; Figure 2b).

[43] Eight earthquakes ($-0.9 \leq M_d \leq 1.5$) were recorded whose epicenters roughly superimpose on the α surface trace. Although hypocenters deepen from east (1–4 km) to west (~ 7 km), epicenters keep plotting on or close to the fault surface trace. If the recorded events result from slip on or close to the α fault planes, we infer that those are steep, dipping south by $80 \pm 5^\circ$ down to 3–7 km. This is in keeping with the three calculated focal mechanisms that reveal normal slip on $N105 \pm 10^\circ E$ subvertical planes (Figure 6a).

4.2.4. Fieale Area, Broad Sense

[44] The greatest density of seismicity is found in the easternmost part of the subaerial rift inner floor, in the $\sim 15 \text{ km}^2$ “Fieale area” (Figure 2). The Fieale caldera is surrounded by a steep, 20- to 30-m-high, ~ 1.5 -km-diameter rim. It is connected to two smaller calderas, the “f” caldera to the south, and the Shark Bay caldera to the east (Figures 2 and 5a). The three volcanic edifices are likely to be fed by the same magmatic source at depth. All are cut by a dense network of approximately E–W to NW striking open fissures and small normal faults. The major one is the south facing B fault system that cuts the Fieale caldera to the north. The B and D scarps face each other and bound a NW trending graben that narrows and tapers westward to end at the eastern termination of the axial volcanic chain. The Fieale caldera is almost entirely enclosed in that graben, so that it is subsiding overall (Figures 2 and 5a).

[45] The 145 events recorded in the Fieale area gather in a few major clusters with few if any events in between (Figures 5a and 6b). The denser cluster overlays the Fieale caldera. Another group of events is identified in the Shark Bay caldera area. Most remaining events are distributed in the F caldera area and along the D surface fault trace.

[46] The epicenters overlying the Fieale caldera form two distinct groups, which are clearly separated in along-strike cross section (Figures 5g and 6b). The first group includes ~ 30 events ($-1.0 \leq M_d \leq 1.2$) whose epicenters roughly overlay the western section of the caldera rim, between faults D and B. The second group includes ~ 70 events ($-1.0 \leq M_d \leq 2.5$) whose epicenters overlay the eastern section of the caldera rim, again between faults D and B.

[47] Hypocenters of the first group of events form a vertical alignment superimposing on a section of the western discontinuity identified between the central low-velocity column and the surrounding high-velocity cylinder (Section 4.1 and Figure 5g). Their focal depths range between 2.5 and 4.2 km with most events concentrated at ~ 4 km. The particular distribution of events along the western discontinuity suggests that they may result from slip on that discontinuity, which we infer to be a brittle shear plane. Together with the fact that the discontinuity extends right below the western Fieale caldera rim and separates volumes of distinct “nature”, this suggests that the western discontinuity is a ring fault. Note that ring faults are common features in volcanic edifices. They generally have curved planes (in map view) that may be vertical, inward or outward dipping [Mori and McKee, 1987; Ekström, 1994; Lipman, 1997; Roche et al., 2000; Lagabrielle et al., 2001; Acocella et al., 2000; Prejean et al., 2003; Gray and Monaghan, 2004;

Folch and Marti, 2004; Cole et al., 2005]. The ring fault inferred on the western side of Fieale is likely to have a subvertical plane, i.e., oscillating from slightly inward to slightly outward, on which both normal and reverse slip events may occur. Seventeen focal mechanisms were determined in this zone (Figure 6b). Seventy percent are DC and indicate normal and strike-slip faulting on steep N–NW to N–NE striking planes. The remaining mechanisms are NDC, with four fifths revealing tensile cracking on NE striking planes. All mechanisms are thus compatible with ruptures on or close to the main, subvertical, NE trending western Fieale ring fault. The existence of various mechanisms (normal, strike slip, NDC) may result from local perturbations of the stress field in the volcanic conduit [e.g., Troise et al., 1997]. We will come back to this point in discussion. Finally, the lack of seismicity on the ring fault at a depth $> \sim 4$ km suggests that the recorded events may have occurred at the ring fault base (Figure 5g).

[48] Hypocenters of the second group draw a more compact cluster between 2 and 3 km depth (Figures 5a and 5g). That cluster is located directly below the likely extension at depth of the eastern section of the Fieale caldera rim. Along with the fact that the event epicenters roughly underline the curved base of the caldera rim at the surface (Figure 6b), this suggests that the second group of events result from slip on an eastern, subvertical, Fieale ring fault (Figure 5g). Since no events are recorded further below the cluster, the second group of events may attest to ruptures at the downward tip of the eastern Fieale ring fault. Most focal mechanisms calculated for events in this area are similar to those found further west, i.e., they attest to both normal and strike-slip faulting or to tensile cracking on steep N–NE striking planes, roughly parallel to the eastern caldera rim and inferred ring fault (Figure 6b). The remaining mechanisms reveal normal slip on steep (preferred focal planes), $N120 \pm 10^\circ$ striking planes parallel to the major normal faults that dissect the Fieale caldera. As most events showing these mechanisms have their epicenters located close to either D or B surface fault traces (and in these fault hanging walls), they are likely to attest to slip on or associated with these two faults. We infer that D and B faults have steep planes at least down to 3–4 km (Figures 5d and 5e).

[49] Only a few events are found between the two major clusters described above. They plot at ~ 3 km depth in the center of the Fieale caldera, still between the surface traces of faults D and B (Figure 6b).

[50] Observed on an along-strike cross section, all Fieale events gather in a ~ 1 -km-thick and 1- to 1.5-km-wide volume that appears as a lens of brittle material capping the western half of the central, low-velocity, aseismic column (Figure 5g). The lens seems to dip by 30 – 50° toward the northwest (stippled lines in Figure 5g). That brittle volume is even clearer on a perpendicular cross section (Figures 5d and 5e); events cluster in a ~ 1 -km-thick and ~ 1.5 -km-wide volume enclosed by the subvertical D and B fault planes. The latter are likely to be responsible for some of the events. The brittle volume seems to dip gently southwestward (20 – 30°) at the top of the central, low-velocity, anomaly column.

[51] Events recorded in the Shark Bay caldera area share similarities with the Fieale events. Most have hypocenters at

2–3 km depth, while most epicenters circle the caldera (Figures 5a–5g and 6a). All events are also enclosed between the D fault and a northern limit that would coincide with the eastward prolongation of the B fault system. On an along-strike cross section, the Shark Bay events draw a SE dipping ($\sim 45^\circ$) elongated cluster capping the eastern half of the low-velocity central column, between the Fieale eastern ring fault and the sharp, subvertical discontinuity identified below the eastern part of the Shark Bay caldera. As in Fieale, some of the events superimpose on that discontinuity, suggesting that they may result from slip on it. We interpret the discontinuity as a ring fault that bounds the whole Fieale-Shark Bay (Fieale-SB) volcanic system to the east (Figure 5g). Focal mechanisms determined for some of the events reveal both normal faulting on steep, E–W to NW striking planes, and more complex mechanisms (strike slip and normal, and one reverse) on various planes oblique to the rift (Figure 6a).

[52] The few events recorded between the F and D surface traces mainly underlay the F cone (Figures 5a and 6a). Their epicenters underline the NE elongated caldera, while their hypocenters cluster at ~ 3 km (Figures 5d and 5e). They are bounded to the south by the F fault plane. If some of the events result from slip on or close to this plane, we infer F to dip steeply northeastward (Figures 5d and 5e). That the events recorded in this zone spread at the same overall depth as those in Fieale suggests that they may result from processes similar to those depicted in the Fieale brittle volume. Events are too sparse, however, for definite conclusions to be drawn.

[53] Taken together, the Fieale and Shark Bay events cluster in a ~ 3 km³ ($1 \times 1.5 \times 2$ km³) volume of brittle material that caps the central column of negative anomaly (Figure 5g). That volume includes two lenses dipping in opposite direction away from the Fieale eastern ring fault. While some events within the lenses likely result from slip on D and B and possibly other smaller faults in between, most attest to ruptures at the base and between the Fieale and Shark Bay caldera ring faults. As these ruptures occur above the central column of velocity anomaly, they may well be related to this particular zone.

4.3. Space-Time Evolution of Seismicity

[54] Although our experiment only lasted for 5 months, it allowed recording all the events that occurred within the network with a magnitude down to -1.0 . This complete and continuous recording offers the opportunity to examine the temporal evolution of seismicity (Figures 7–9).

[55] Seismic activity was irregular over time (as observed in other volcanic environments [e.g., *Parson et al.*, 1993; *Canales et al.*, 2000; *Tolstoy et al.*, 2001]), varying at least by two different timescales. It first varied at a scale of several weeks (Figure 8). During the first 5 weeks of recording (dark violet), most events occurred in the southern part of the rift inner floor, while the rift remained quiescent north of its axis (with the exception of the ε system). During the following 4–5 weeks (pale blue), the situation reversed with most events occurring north of the rift axis while the rift remained quiescent in its southern part. In the weeks that followed (green), activity shifted and spread at the rift axis (Fieale/Shark Bay area) while the rest of the rift became quiescent. Subsequent activity remained in the Fieale area

but was discontinuous. While activity in Fieale essentially started in January 2001, it significantly increased on 27 February (Figures 7a and 8). Eighty events were produced between that day and the end of the experiment, all below the Fieale caldera. That several week long Fieale sequence was therefore a major phase in the rift activity.

[56] During each of the several week periods described above, seismic activity also varied at a shorter timescale, varying from a few minutes to a few days. Most events indeed occurred in short swarms (which we refer to as “crises” hereafter; Figures 7a and 8), each producing a large number of events in a narrow volume. Where they repeated (as in Fieale), the crises were separated by time spans much longer than their duration.

[57] Below we describe in greater detail the main periods of activity mentioned above. As the Fieale sequence is a major phase, we analyze the seismicity before and during that phase separately.

4.3.1. Activity Before the Fieale Sequence

[58] Figures 9a–9d show both in map and cross sections the events that occurred before the Fieale sequence, with colors indicating their temporal evolution. One hundred thirty-eight events were recorded before the Fieale sequence (from 20 October 2000 to 26 February 2001). The general picture of this period shows a somewhat distributed seismicity (Figure 9a): Events occurred in all zones previously described (section 4.2). In more detail, seismic activity occurred through a succession of crises that affected spatially distinct volumes. Most crises did not repeat in similar ways. Finally, the occurrence of any crisis was accompanied by an almost complete cessation of activity elsewhere in the rift. The ε fault system is the only feature to show “continuous” activity during this first phase, and actually throughout the entire experiment (Figure 8).

[59] A first crisis occurred at the end of October 2000 (Figures 7a, 8, and 9a, dark violet). Twenty-five events were recorded in 10 days, most in the hanging wall of the D fault and underlining its scarp base. This suggests that the October activity was produced by slip on D or on associated rupture planes. The focal mechanisms determined for some of these events are consistent with this inference (Figure 9). They show steep (preferred) planes whose strikes vary from W–NW to N–NW as one goes from SE to NW, as does the D surface trace. That these planes dip slightly opposite to the D scarp suggests that the D fault has a subvertical plane at least down to 3–4 km. The left-lateral component revealed to the NW is compatible with the long-term kinematics of the fault (see *Manighetti et al.* [1998] and *Manighetti* [1993] for details).

[60] Seven events occurred the first 15 days of December in a small zone at the base of the $\alpha 1$ fault scarp (blue, Figure 9a). The focal mechanisms calculated for some of these events suggest that this cluster results from slip on $\alpha 1$, which is interpreted as having a steep ($\sim 80^\circ$) plane at least down to 3–4 km.

[61] Another crisis occurred in December 2000 (10–31 December, Figures 7a and 9a, blue green). It produced 16 events clustered within the DLM inner floor. These events apparently resulted from tensile cracking, as discussed before (section 3.5).

[62] On 9 January, another crisis occurred which produced a swarm of 17 events S–SW of the Shark Bay caldera

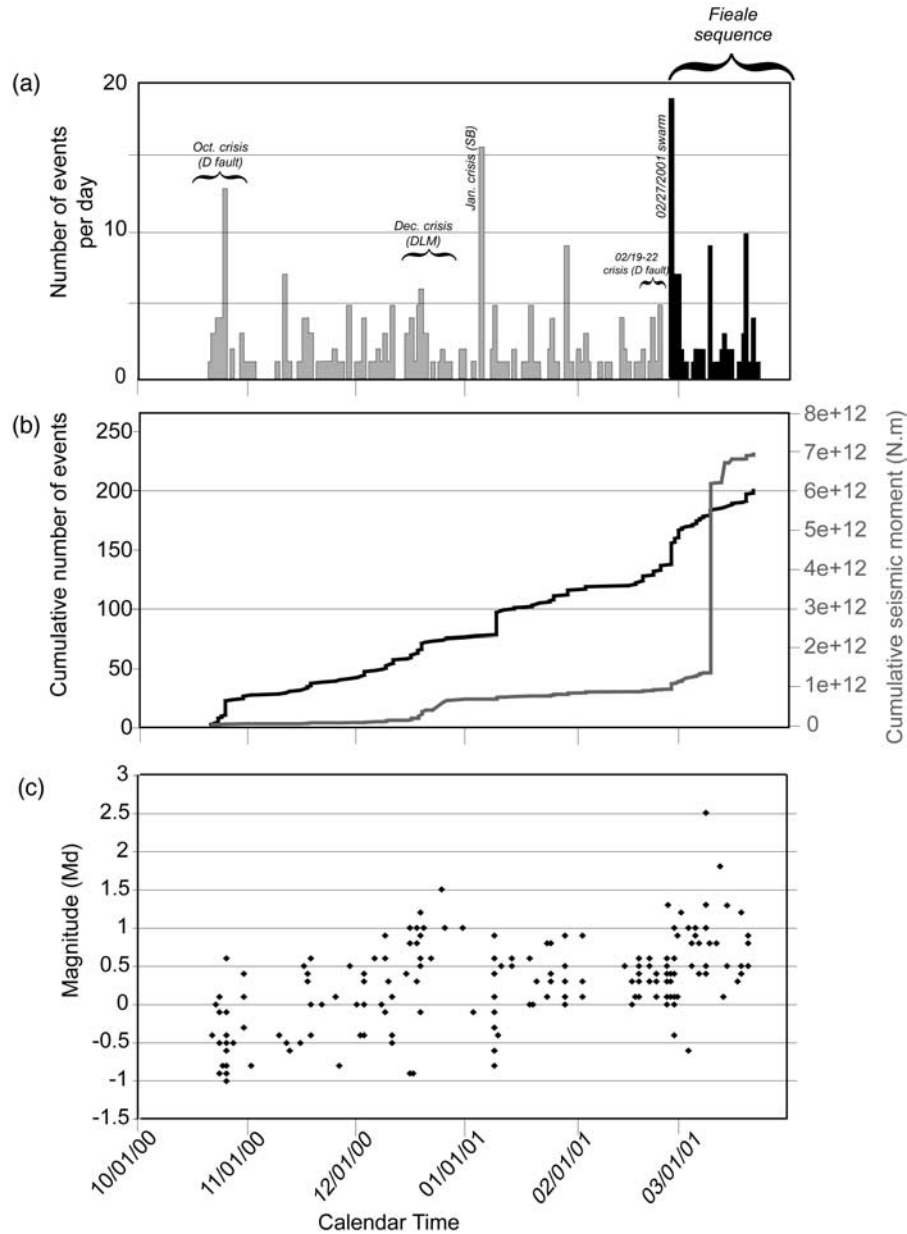


Figure 7. (a) Time evolution of daily number of events, (b) cumulative number of events (black curve), cumulative seismic moment (gray curve), calculated from formula of *Kanamori and Anderson* [1975]), and (c) event magnitudes. In Figure 7a, the Fieale sequence is in black while major crises before that sequence are indicated.

(Figures 7a, 8, and 9a; dark green). Together with a few subsequent events, the swarm draws a semicircular pattern that underlines the base of the volcanic edifice. This suggests that the January crisis attests to ruptures on or around the Shark Bay caldera ring faults (Figure 9d). However, most focal mechanisms determined in the Shark Bay area reveal normal to normal-left-lateral slip on E–W to NW striking, steep planes, parallel to the small faults and fissures that dissect the area. Slip on these planes may thus also account for events in this zone.

[63] Finally, a swarm of eight events occurred between 19 and 22 of February, near the intersection between the D and

the eastern Fieale ring faults (Figures 7a, 9a and 9c; red). Focal mechanisms are similar to those determined for the October crisis events, suggesting that the February swarm mainly attests to slip on or around D, where it intersects the Fieale and F calderas.

[64] Altogether, a total of 48 focal mechanisms were calculated for events having occurred during that first phase of activity. Ninety-one percent of them are double couple (Figure 10a). Most of the solutions indicate normal (14) or normal left-lateral slip (11) on approximately E–W to NW striking, steep planes (preferred solutions). The solutions thus are in keeping with slip on major rift faults (whose

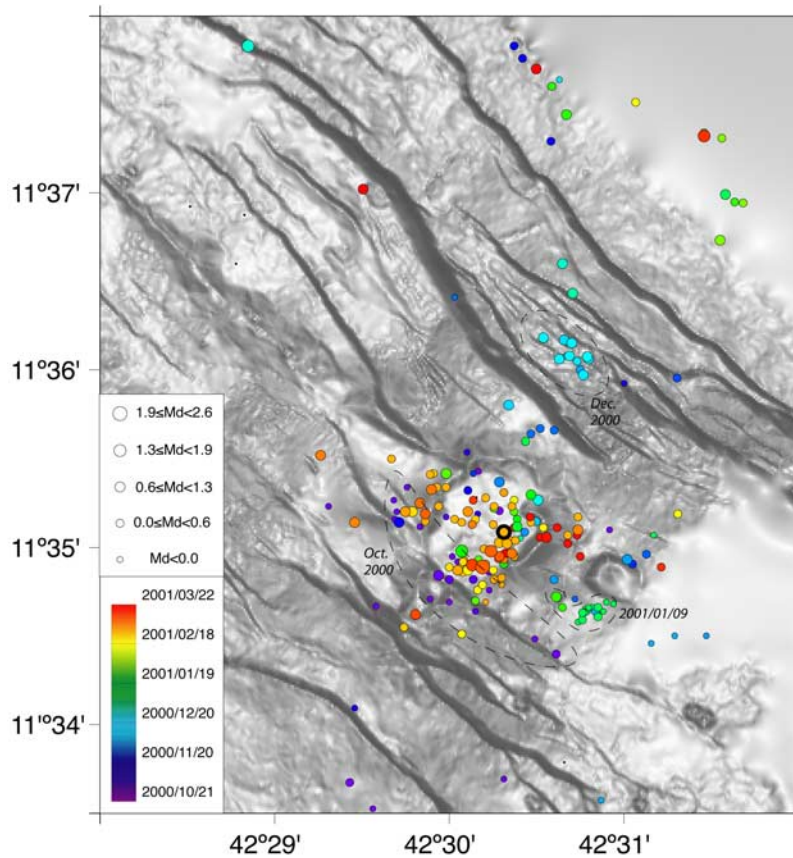


Figure 8. Space-time evolution of recorded events (map view). Major crises are indicated. First shock of Fieale sequence is indicated by black circles.

long-term kinematics is normal and left lateral [Manighetti *et al.*, 1998]). Overall, the T axes of the solutions strike approximately NE (Figure 10a), hence parallel to the regional σ_3 vector [Ruegg and Kasser, 1987; Vigny *et al.*, 2007]. This leads us to conclude that most events result from slip on the rift faults, and occurred in a homogeneous extensional stress regime, similar to the regional one. Event distribution furthermore indicates that the fault systems ϵ , α_1 , B, and D were the most active during this first period of time. The few remaining focal solutions reveal reverse, normal, or lateral slip on planes with various strikes oblique to the rift. They are also compatible with a NE trending direction of extension, however.

[65] Thus before the Fieale sequence, seismic activity was mainly tectonically accommodated, resulting from slip on, or microrupturing around, the central northern major rift faults, in a homogeneous regional extensional stress regime. Faults, however, only slipped in the eastern emerged part of the rift in close proximity to the Fieale volcanic edifice.

4.3.2. Activity During the Fieale Sequence

[66] Figures 9e–9h are done as before for the events that occurred during the Fieale sequence.

[67] The Fieale sequence started at 15:48 on 27 February 2001 with a $M_d = 1.3$ shock within the caldera (black circled in Figures 8 and 9e), was then followed by 17 more events on that day and 62 over the next 23 days (Figure 7a). Note that we had to interrupt the experiment before the end

of the Fieale sequence. However, the permanent network could record it till July 2001 (Arta Observatory Staff, personal communication, 2006). The sequence only struck the Fieale caldera area, while the rest of the rift remained quiescent. Events almost exclusively occurred in the inner floor of the B-D subsiding graben, and between the Fieale caldera ring faults. They were produced during successive short crises that followed more frequently than ever before (Figure 7a). These crises affected spatially distinct volumes, none of which had broken during the first phase. More, the Fieale sequence events roughly filled the gaps that had been left free of earlier events. This makes the Fieale events basically clustering in the central part of the Fieale caldera, hence at the rift axis, quite far (~ 800 m) from the B and D faults. Those are thus inferred not to have slipped significantly during the Fieale sequence.

[68] The sequence started with a first crisis (violet, Figure 9e) during which 18 events were produced below the Fieale caldera. The very first event occurred at the base of the eastern ring fault (Figures 9e and 9h). The subsequent events spread westward in the interior of the west dipping, brittle volume depicted at the top of the central, low-velocity column. Taken together, the epicenters form a NW trending alignment at the rift axis.

[69] A little more than a week later, another crisis produced seven events (green, Figure 9e), the first few at the base of the eastern ring fault, and the later ones within

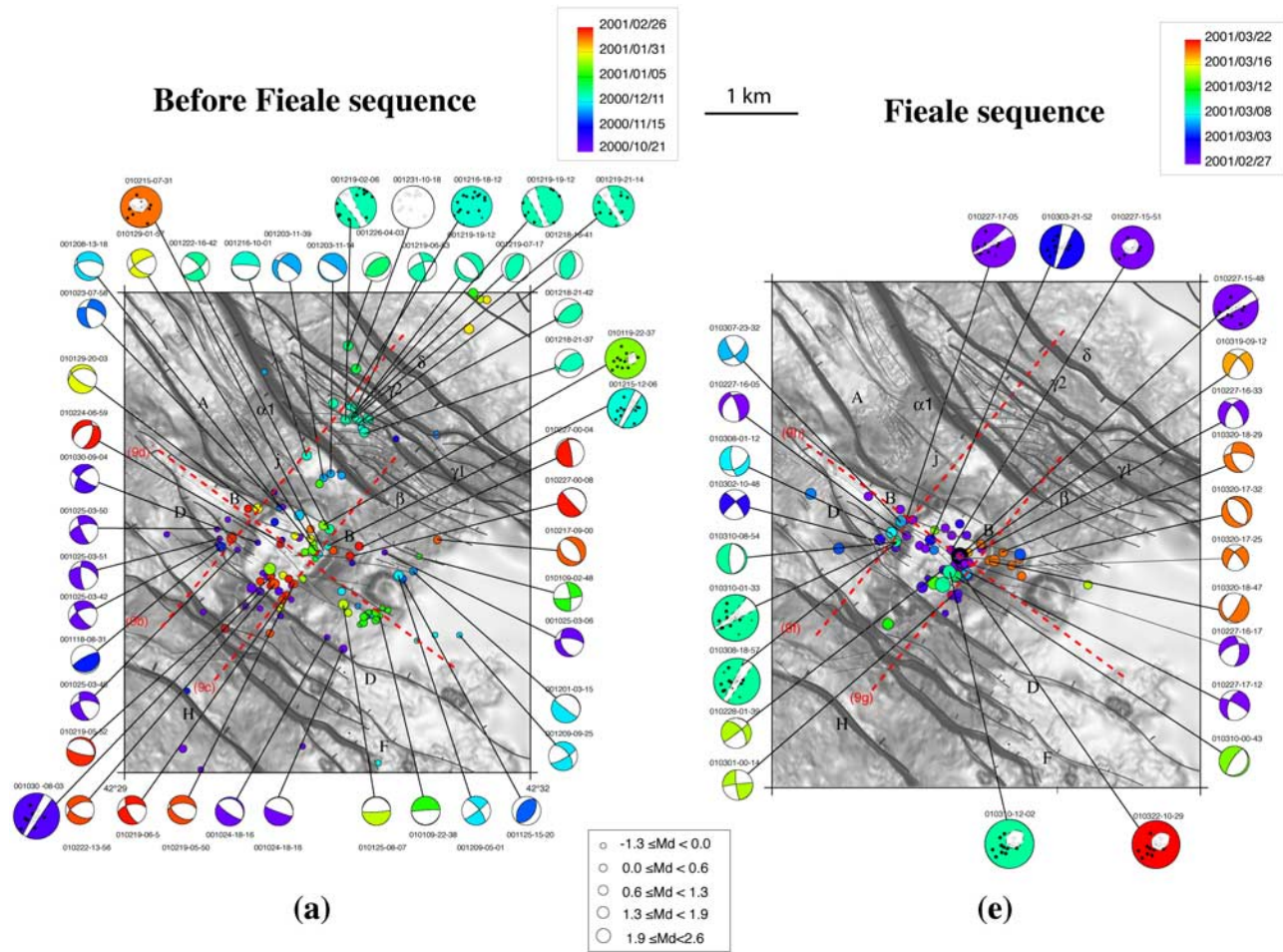


Figure 9. Events and focal mechanisms (a–d) before and (e–h) during the Fieale sequence. Structural maps and cross sections as before (cross sections are located in Figures 9a and 9e). Events in northern shoulder are omitted for clarity. In Figures 9b–9d and 9f–9h, focal solutions are in planes of cross sections. In Figures 9e, 9g, and 9h, the very first event is black circle.

the brittle lens and on the western ring fault (Figures 9e and 9h) A little more than a week later another crisis occurred (orange, Figure 9e) with events stretching from the western Shark Bay ring fault where they seem to have initiated, to the eastern Fieale ring fault where they seem to have ended.

[70] Overall, a total of 24 focal mechanisms were calculated for some of the Fieale sequence events. Sixty-seven percent are double couple and characterized by an E–W trending T axis (Figure 10b) oblique to the direction of regional extension. Most indicate normal slip on rather steep planes (~ 70 – 85°) striking $N0 \pm 25^\circ$ (Figure 10b). As faults striking N–S are not observed in the rift, the corresponding events are unlikely to result from slip on some of the rift faults. The events whose epicenters underlie surface fault traces show nodal planes that are actually oblique to these traces, hence incompatible with slip on these faults. By contrast, the Fieale caldera ring faults, at the base of which most events occur, strike N–S to NE–SW on average where events are denser (Figure 9e). Along the NE trending section of the eastern Fieale ring fault, most mechanisms show a subvertical or steep, west dipping, NE striking focal

plane, consistent with slip on that ring fault. Similarly, along the NE trending section of the western Fieale ring fault, most mechanisms show a subvertical or steep, east dipping, north to NE striking focal plane, consistent with slip on that ring fault. Together these suggest that most Fieale events result from frictional ruptures on or around both western and eastern Fieale ring faults at depth, where those are enclosed between the B and D fault planes. Most remaining DC mechanisms indicate strike-slip faulting on steep planes with various strikes. Nine NDC mechanisms are also found that reveal explosion/implosion and tensile cracking mechanisms.

[71] We conclude that the Fieale sequence was mainly magmatically accommodated and possibly induced. Ruptures basically occurred at the base of the Fieale ring faults and within the brittle lens that caps the central column of low-velocity anomaly. Moreover, they are characterized by a E–W trending T axis, suggesting that they occurred in a local stress regime different (i.e., rotated by $\sim 45^\circ$) from the regional one. We suggest that this particular stress regime resulted from a local perturbation of the regional stress

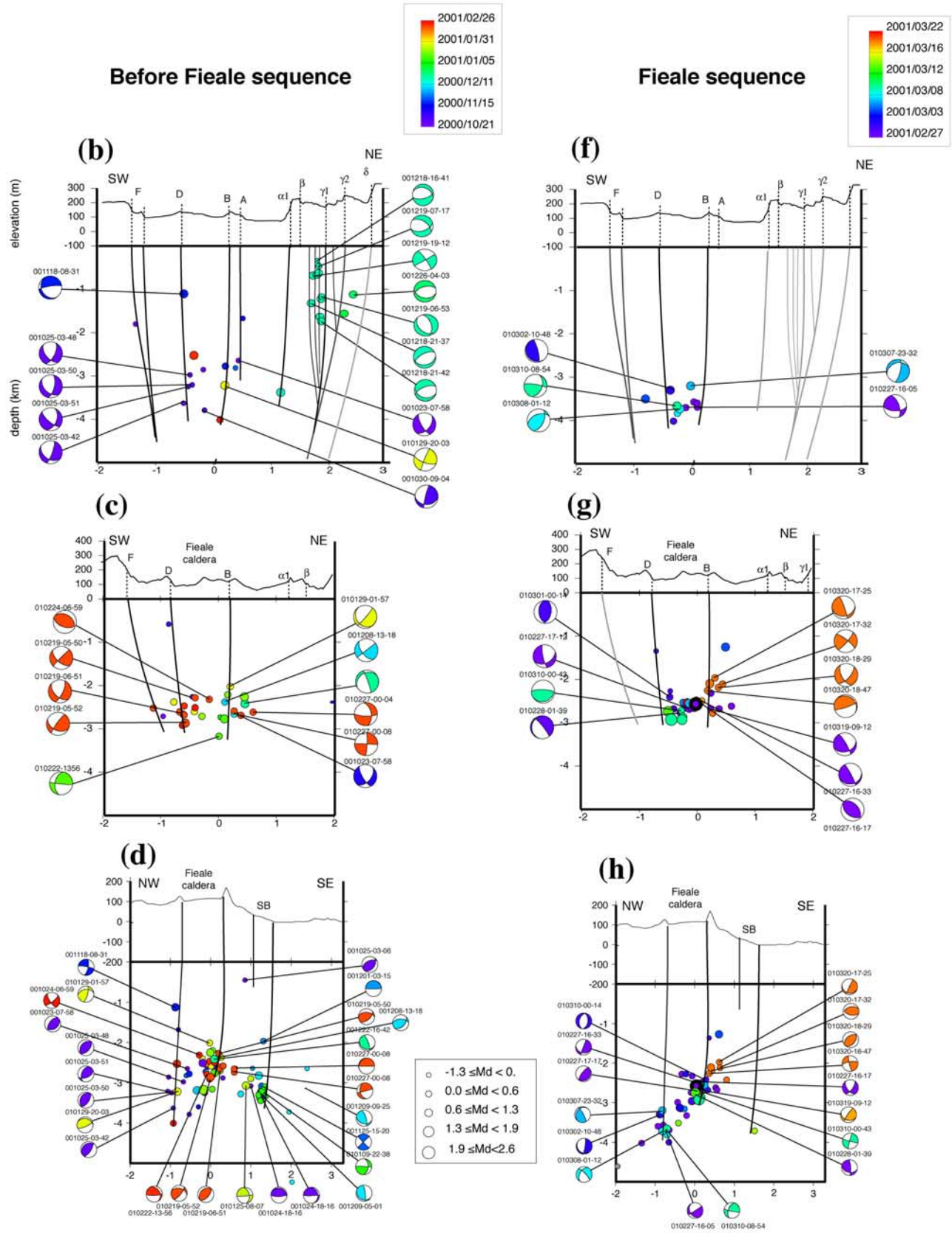


Figure 9. (continued)

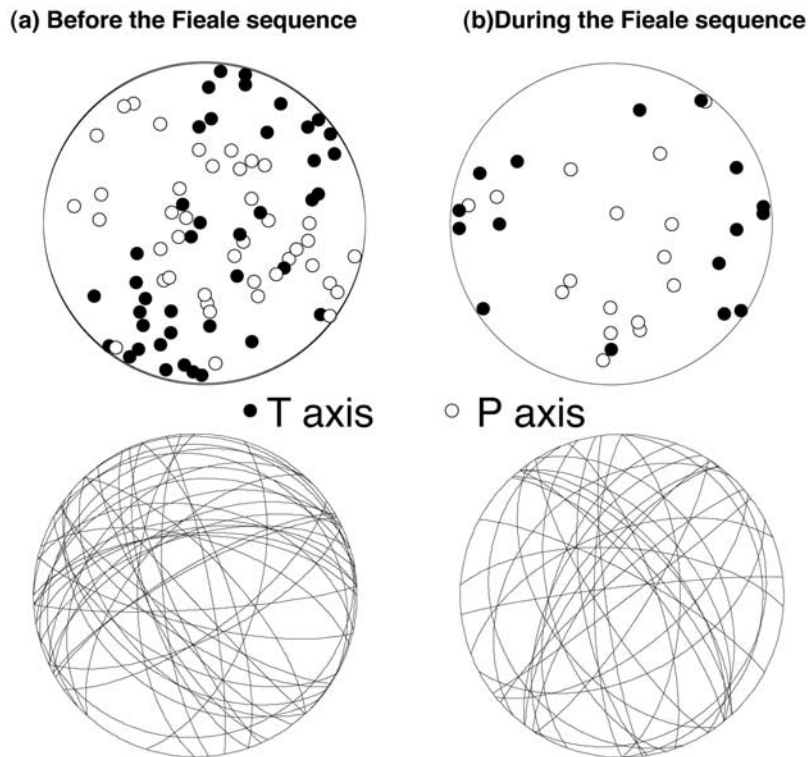


Figure 10. Stereographic projection of (top) P and T axes and (bottom) nodal planes of double-couple focal mechanisms determined for events (a) before and (b) during the Fieale sequence.

environment as a response of a sudden change in the magmatic activity below the Fieale caldera.

5. Discussion

5.1. Shallow Crustal Structure in the Subaerial Section of the Rift

[72] The recorded data help depicting the shallow crustal structure in the onland section of the rift, especially in the area of Fieale. Note that before the present study, little was known on that structure. In particular, though a magma chamber is suspected somewhere below the Fieale edifice [Van Ngoc *et al.*, 1981], its depth, geometry, composition, internal magma pressure, relationships to Fieale and to faults, etc., are unknown. Similarly, though the Fieale volcano is a major feature of the rift, its geometry at depth, its possible role in the rift plumbing system, etc., are unknown. We thus feel that our results bring valuable insights to characterize the rift structure and behavior. Our vision of the rift structure and behavior is conceptualized in Figure 11 of the companion paper by Doubre *et al.* [2007], once all available data have been analyzed. Here we thus only report major observations and inferences issued from that first part of work.

[73] As discussed by Gudmundsson *et al.* [1994] and Arnott and Foulger [1994a], the variations of seismic wave velocities in volcano-tectonic environments likely result from temperature variations and/or variations in rock porosity or density. Temperature variations are generally related to the existence of a magmatic plumbing system and/or to fluids circulations. Porosity anomalies are most

likely associated with the existence of porous bodies and/or with pervasive fracturing of the rocks.

[74] The central pipe-shaped zone of low velocity that is imaged from 1–2 km down to at least 5 km stands right below the Fieale-Shark Bay volcanic complex, hence about where a long-lived magma chamber is suspected [Van Ngoc *et al.*, 1981]. The amplitude of the anomaly is too low, however, to attest to the presence of molten basaltic material; such material would produce P wave velocity anomalies >1 km/s [e.g., Gudmundsson *et al.*, 1994]. It is by contrast similar to the P wave anomaly found at the roof of the Krafla magma chamber [Brandsdottir *et al.*, 1997] and interpreted as resulting from a temperature increase in solid rocks above the reservoir. The lack of earthquakes in most of the low-velocity pipe (below 3–4 km) suggests that temperatures in the pipe are too high for brittle ruptures to occur. In common conditions, the transition between brittle and plastic rock deformation occurs at 600–800°C, while basaltic rocks start melting at 1150–1350°C [e.g., Cowie *et al.*, 1993; Hirth *et al.*, 1998]. We thus suggest that the axial low-velocity pipe imaged below the Fieale-Shark Bay calderas is a zone of increased temperature with little or no melt above a deeper magma reservoir. Similar low-velocity zones have been recognized above magma reservoirs in other rift or ridge segments, and similarly interpreted [Brandsdottir *et al.*, 1997; Barclay *et al.*, 1998; Dawson *et al.*, 1999; Miller and Smith, 1999]. Temperatures in the pipe are likely to range between 600 and 1200°C below 3 km (down to at least 5.5 km), making the zone essentially made of solid basaltic rocks deforming plastically, thus aseismically. That no similar low-velocity zone is found elsewhere in the subaerial part of the rift

suggests that the magma reservoir is strictly localized below the Fieale-SB calderas, and hence small in size.

[75] The pipe of hot rocks is bounded by the outer ring faults of the Fieale-Shark Bay volcanic system, and enclosed within a large, cylinder-shaped zone of positive anomaly. That cylinder of high velocity is free of earthquakes. Together these suggest that the “cold cylinder” is an annulus of dense, frozen magmatic intrusions, similar to those commonly observed around magma chambers [Arnott and Foulger, 1994a, 1994b; Gudmundsson et al., 1994; Barclay et al., 1998; Miller and Smith, 1999; Dawson et al., 1999]. This inference is in keeping with the large positive gravity anomaly (>2 mGal) measured in the Fieale-Shark Bay area [Demange and Puvilland, 1990]. The annulus of intrusions is likely to form the Fieale-Shark Bay caldera rim at depth.

[76] West of Fieale, the axial volcanic chain is underlined by a zone of negative velocity anomaly that extends from surface down to 3–4 km. Although this zone is poorly resolved, it is consistent with the existence of recent (1978 magmatic episode), still hot, planar intrusions, as with the high temperatures measured in this area (800–1200°C [Van Ngoc et al., 1981]). If the positive anomaly zone evidenced at greater depths is real, we infer that the volcanic chain is not presently fed by ascending hot material.

[77] While P velocity anomalies at depth are likely related to the Fieale magmatic system, those determined in the shallow levels (≤ 1.5 km) may have different origins. For instance, cold seawater infiltrates the onland section of the rift from the Ghoubbet and flows westward through its dense network of faults and fissures up to the Asal Lake [Mlynarski and Zlotnicki, 2001; Demange and Puvilland, 1990; Van Ngoc et al., 1981]. That circulation is confined to the top 500 m [Van Ngoc et al., 1981]. It generates temperature variations that draw an alternation of NW–SE stripes [e.g., Mlynarski and Zlotnicki, 2001]. These stripes, however, are not observed in Figure 4, suggesting that the water-related temperature variations are small. On the other hand, the existence of numerous fumaroles within the Fieale area and along the D and F fault systems attests to significant hydrothermal activity [Demange and Puvilland, 1990; Abdallah, 1997]. Shallow circulation of hydrothermal fluids may thus be responsible for some of the shallow negative P anomalies. Intense, pervasive fracturing also occurs in the rift, particularly in the DLM subrift and at major fault tips [Manighetti et al., 2001a, 2004]. Such pervasive fracturing may thus also account for some of the shallow negative anomalies.

5.2. Seismic Evidence for Tectonic Activity in the Rift

[78] The combined analysis of event distribution, time evolution and focal mechanisms, suggests that faults D, B, α , $\gamma 1-2$, and $\varepsilon 1-2$ are currently slipping and/or embedded in volumes sustaining current brittle deformation. Shallow fissuring is also occurring in the inner floor of the Disa Le Mallo subrift. Most recorded events are enclosed and bounded by the D and B fault planes, suggesting that the latter two faults may be the most currently active in the rift. The normal slip events detected on their planes show that the rift inner floor, hence the Fieale caldera, are presently subsiding. These results are in keeping with geodetic measurements that show that the rift inner floor has been

subsiding at 1–4 mm/yr in the last 20 years in the Fieale area [Ruegg and Kasser, 1987; Doubre et al., 2005; Vigny et al., 2007].

[79] The faults on or around which microevents are detected share several characteristics. First, they all lie in the northern half of the rift (from D to ε). Faults further south show little or no evidence of current activity. This observation seems to confirm that the locus of current tectonic activity is north of the rift axis, particularly in the DLM subrift, as previously inferred from analysis of long-term faulting [Manighetti et al., 1998], and suggested by geodetic measurements [Vigny et al., 2007; Doubre and Peltzer, 2007]. Second, faults only sustain sparse, small ($0.5-1$ km²) clusters of events which, at most, represent total seismic moment of a few $10^{11}-10^{12}$ N m per fault. Thus, if slip occurs on the faults, it is not larger than a millimeter. It is actually more likely that the event clusters rather result from microscale damage fracturing of the rocks embedding the fault planes [e.g., Manighetti et al., 2004].

[80] Another characteristic shared by the seismically active faults is their steep planes. Event distribution and focal mechanisms combine to reveal planes almost vertical down to several km. The D and B fault planes are the steepest, dipping by $85 \pm 5^\circ$ down to 3–4 km. The $\alpha 1$ and F faults seem to have planes almost as steep, dipping by $80 \pm 5^\circ$ down to 3–4 km (and possibly 6 km for $\alpha 1$). Although events occur only at shallow levels, fault planes in the DLM subrift seem also subvertical, and associated with vertical, open fissures. Finally, $\varepsilon 1$ and $\varepsilon 2$ fault planes dip by $50-70^\circ$ SW down to 5–6 km. Although these values are deduced from few events (they will be refined in following paper), they suggest that most rift faults are steep, with dips decreasing from about vertical at the rift axis to $50-60^\circ$ in the oldest, outermost parts of the rift, as observed in oceanic spreading segments [e.g., Kong et al., 1992; Barclay et al., 2001]. This makes most rift faults unable to accommodate large extensional components. More, faults at the rift axis can only accommodate up and down motions of the inner floor and of its embedded Fieale caldera. Finally, the focal mechanisms determined for some of the fault slip events show that faults are slipping or sustaining brittle deformation in a homogeneous regional stress regime consistent with the approximately NE trending direction of the Arabia-Africa plate motion vector. Most of these events show dominant normal slip, while a few others have an additional component of left-lateral slip, as observed in long-term fault kinematics.

[81] The results above demonstrate that tectonic faulting currently occurs in the rift. Yet, it does not efficiently contribute to the rift opening. This is in keeping with observation that total contribution of fault strain to plate separation is low, less than 20%, in most oceanic ridge segments [e.g., Forsslund and Gudmundsson, 1991; Cowie et al., 1993; De Chabaliér and Avouac, 1994; Escartin et al., 1999; Ebinger and Casey, 2001; Behn et al., 2002].

5.3. Seismic Evidence for Magmatic Activity in the Rift

[82] The main evidence of recent magmatic activity comes from the identification of a pipe of hot rocks below the Fieale-Shark Bay volcanic complex. The pipe overlies a magma reservoir that we infer to be at a depth >5 km, in the southeastern part of the Fieale-Shark Bay complex.

[83] Current magmatic activity in the rift is also attested by the distribution and nature of most events. The denser seismicity is found in the Fieale-Shark Bay area, with most events occurring at the base of the Fieale ring faults, and attesting to their slip (or to tensile cracking around them). Clustering of microevents on volcanic ring faults and particularly at their base is a common feature in volcanic areas [Einarsson, 1991; Ekström, 1994; De Natale *et al.*, 1995; Mori *et al.*, 1996; Nettles and Ekström, 1998; Prejean *et al.*, 2003; Sohn *et al.*, 2004]. Another common feature is that microevents tend to form dense clusters at the top of magma reservoirs [e.g., Nicolas *et al.*, 1993; Sohn *et al.*, 2004]. In our case, events rather cluster at the top of the hot rock pipe, hence more than 2–3 km away from the reservoir roof. We suggest that the reverse V-shaped volume that the cluster forms, is made of extrusive rocks, now frozen at the roof of the hot pipe. The brittle volume is enclosed within the ring faults and the D and B fault planes, and likely slide up and down along them. Its reversed V shape suggests that the extrusive lenses are tilted outward as a response of an upward “magmatic push” from underneath (inflation; e.g., Brandsdóttir and Einarsson, 1979; Tryggvason, 1986; Tait *et al.*, 1989; Tilling and Dvorak, 1993; Dawson *et al.*, 1999]. The NDC mechanisms found in the volume may therefore result from both thermal (contraction/dilation of rocks) and pressure effects.

[84] Finally, the temporal evolution of seismicity also attests to current magmatic activity in the rift. A several week long period is identified (Fieale sequence), during which events only occur in the Fieale area, with mechanisms significantly different from those observed in “rest conditions”. This strongly suggests that the Fieale sequence occurs in a modified stress regime (rotation of $\sim 45^\circ$ of the strike of the extensive stress axis). That modified regime likely results from a local stress field interacting and adding to the regional stress field. We take that local stress perturbation to result from a sudden pressure change in the Fieale magma reservoir and overlaying hot pipe. Note, however, that thermal stresses might also be high enough to contribute modifying the ambient stress regime [e.g., Chevallier and Verwoerd, 1990; Gerla, 1988].

[85] The results above demonstrate that magmatic activity is currently going on in AG, in the Fieale-Shark Bay area. Yet, it does not contribute either to the rift opening, for most of its “effects” are small, up and down, vertical displacements on the Fieale-SB volcanic ring faults.

5.4. Seismic Evidence for Current Magmato-Tectonic Interactions in the Rift

[86] The experiment shows that tectonic and magmatic processes currently interact in the rift, with these interactions governing the time-space evolution of seismicity. First, the recorded events spread in a few zones that all (but ε) are in the vicinity of the Fieale caldera; they lie within a ~ 2 -km-wide, ~ 5 -km-long, NE trending strip that runs from Fieale to $\varepsilon 2$. Anywhere else outside of this “seismic strip”, the rift is quiescent. This particular distribution suggests that the current activity, including that on faults, is somehow related to the Fieale volcanic system. Second, phases of peaked activity are identified at different timescales; whenever and wherever such a phase of peaked activity occurs, it inhibits the activity in the rest of the rift. More, a major

phase of peaked activity in Fieale-SB (Fieale sequence) locally disturbs the ambient stress regime. We take that Fieale sequence to result from a pressure change in the magma reservoir underneath. Although small, the perturbation is sufficient to impede adjacent volumes and faults to deform or rupture. This demonstrates that magmatic and tectonic activities currently interact. This further shows that as elsewhere, the Fieale volcanic source and its adjacent faults (including ring faults) are mechanically coupled through two-way stress transfers [Pollard *et al.*, 1983; Rubin, 1990; De Natale *et al.*, 1995; Gudmundsson, 1998; Burov and Guillou-Frottier, 1999; Troise *et al.*, 2003; Doubre and Geoffroy, 2003; Feuillet *et al.*, 2004, 2006; Gray and Monaghan, 2004]. That the Fieale sequence inhibits slip on adjacent faults suggests that it results from a pressure increase. It also suggests that at the time of the experiment, σ_3 was hardly lower than σ_1 and σ_2 for its small increase was enough to “reset” the ambient stress regime and lock the faults. The ambient stress regime may thus have been close to isotropic.

6. Conclusions

[87] The 5-month seismological experiment that we conducted in the Asal-Ghoubbet Rift allowed the continuous recording of events down to a magnitude of -1.0 . We ended locating 208 events in the rift ($-1.0 \leq M_d \leq 2.5$), 200 of them occurred within the temporary network, i.e., in the eastern emerged part of the rift. These events were dense enough to be used in a tomographic inversion procedure, from which we inferred the crustal structure of the eastern part of the emerged rift, and relocated the events with a precision of a few tens of meters. Focal mechanisms could also be determined for a large number of events (71). Altogether, the data allowed event nature, distribution and temporal evolution to be examined in great detail, and faced to the main tectonic and magmatic features known at surface and identified in the tomography. Our main findings are the following.

[88] 1. Though the rift is currently opening at 16 ± 1 mm/yr, the level of seismicity recorded over the 5 months is quite low, hardly accounting for a total seismic moment of 7×10^{12} N m. Similarly, although most faults in the rift show morphological evidence of recent to current activity, very few are associated with seismicity.

[89] 2. The recorded seismicity is concentrated in one single zone, the northeastern quadrant of the rift emerged section. The rest of the rift is entirely silent. The zone of seismicity divides in three distinct clusters, coinciding with the Fieale-Shark Bay area (inner floor), the Disa Le Mallo subrift, and the northern rift shoulder. They are all close to the Fieale-Shark Bay volcanic system, below which a magma chamber is suspected.

[90] 3. The tomographic results confirm that the Fieale-Shark Bay area is an important element of the rift plumbing system. The whole caldera zone is found to overlay a ~ 2 -km-wide central column of low-velocity anomaly that we interpret as a pipe of heated rocks above a deeper magma chamber (lying at depth >5 – 6 km). That pipe is enclosed within a cylinder-shaped zone of high-velocity anomaly that we interpret as an annulus of frozen intrusions. The Fieale-Shark Bay caldera rims extend down to 4–5 km through a

system of subvertical ring faults that separate the central hot pipe from the outer intrusion annulus.

[91] 4. Most earthquakes occur at the base of the ring faults (at 3–4 km), where those are enclosed between the vertical, innermost D and B normal fault planes. This makes most of the recorded seismicity forming a dense $\sim 3 \text{ km}^3$ cluster at the roof of the central hot pipe, in between the volcanic and the tectonic faults that bound the Fieale-Shark Bay volcanic system at depth.

[92] 5. Most of the seismicity results from up and down motion on both the volcanic ring faults and the tectonic B and D faults. These up and down motions are likely driven by pressure changes in the magma chamber underneath. One of such pressure change is taken to be the cause of the Fieale sequence, during which a large number of events were produced below the caldera in a short time, while the ambient stress regime was significantly locally modified and apparently reset to almost isotropic.

[93] Taken together, our observations demonstrate that the central Fieale-Shark Bay volcanic complex is currently active, despite the lack of other evidence. That activity seems to result from small pressure changes in a deeper magma reservoir. These pressure changes produce inflation/deflation motions of the brittle lens that caps the overlying pipe of hot rocks. These motions in turn produce small slip events on the shear planes that bound the pipe. If this vision is correct, it suggests that during the experiment, the rift activity was essentially magmatically induced and accommodated, while tectonic faulting was basically silent, or hardly significant.

[94] All these results are refined in the companion paper by Doubre *et al.* [2007], where we examine the evolution of seismicity in the rift over the 23 years that followed the 1978 rifting episode.

[95] **Acknowledgments.** Our deepest thoughts and thanks go to Jean-Louis Cheminée, whose constant help allowed that work to be done and whom we are so much missing. We also thank the Centre de Recherche Scientifique de Djibouti (CERD, Djibouti), especially the directors M. Anis Abdallah and M. Jalludin Mohamed, and the Observatoire Volcanologique de Djibouti (Arta, IPGP-CERD), for their constant collaboration and their scientific and logistic support. We thank the Institut National des Sciences de l'Univers (INSU, France) and the CNRS for their financial support. The installation of the seismological network was made possible with the help of the French Army in Djibouti, which we also thank. We are grateful to N. Muller, J. Sahr, A. Hauser, and M. Frogneux for their technical work and to J. C. Ruegg, G. King, J. B. De Chabaliér, H. Haessler, and L. Geoffroy for fruitful discussions. We are also thankful to S. Prejean, C. Wilson, and two anonymous reviewers whose thorough comments helped to improve the manuscript. Contribution 394 of INSU-France and 2187 of IPG-Paris.

References

- Abdallah, A. (1997), *Champ géothermique d'Asal, République de Djibouti*, thèse de Doctorat, 137 pp., Univ. Denis Diderot, Paris.
- Abdallah, A., V. Courtillot, M. Kasser, A. Y. Le Dain, J.-C. Lépine, B. Robineau, J.-C. Ruegg, P. Tapponnier, and A. Tarantola (1979), Relevance of Afar seismicity and volcanism to the mechanics of accreting plate boundaries, *J. Geophys. Res.*, **89**, 7689–7696.
- Accocella, V., F. Cifelli, and R. Funicello (2000), Analogue models of collapse calderas and resurgent domes, *J. Volcanol. Geotherm. Res.*, **104**, 81–96.
- Aki, K. (1984), Evidence for magma intrusion during the Mammoth Lakes earthquakes of May 1980 and implications of the absence of volcanic (harmonic) tremor, *Nature*, **282**, 17–23.
- Arnott, S. K., and G. R. Foulger (1994a), The Krafla spreading segment, Iceland: 1. Three-dimensional crustal structure and the spatial and temporal distribution of local earthquakes, *J. Geophys. Res.*, **99**, 23,801–23,825.
- Arnott, S. K., and G. R. Foulger (1994b), The Krafla spreading segment, Iceland: 2. The accretionary stress cycle and nonshear earthquake focal mechanisms, *J. Geophys. Res.*, **99**, 23,827–23,842.
- Audin, L., I. Manighetti, P. Tapponnier, F. Métyvier, E. Jacques, and P. Huchon (2001), Fault propagation and climatic control of sedimentation on the Ghoubbet Rift Floor: Insights from the Tadjouraden cruise in the western Gulf of Aden, *Geophys. J. Int.*, **144**, 391–413.
- Ballu, V., M. Diamant, P. Briole, and J.-C. Ruegg (2003), 1985–1999 gravity field variations across the Asal Rift: Insights on vertical movements and mass transfer, *Earth Planet. Sci. Lett.*, **208**, 41–49.
- Barclay, A. H., D. R. Toomey, and S. C. Solomon (1998), Seismic structure and crustal magmatism at the Mid-Atlantic Ridge, 35°N , *J. Geophys. Res.*, **103**, 17,827–17,844.
- Barclay, A. H., D. R. Toomey, and S. C. Solomon (2001), Microearthquake characteristics and crustal V_P/V_S structure at the Mid-Atlantic Ridge, 35°N , *J. Geophys. Res.*, **106**, 2017–2034.
- Behn, M. D., J. Lin, and M. T. Zuber (2002), Mechanisms of normal fault development at mid-ocean ridges, *J. Geophys. Res.*, **107**(B4), 2083, doi:10.1029/2001JB000503.
- Brandsdottir, B., and P. Einarsson (1979), Seismic activity associated with the September 1977 deflation of the Krafla central volcano in northeastern Iceland, *J. Volcanol. Geotherm. Res.*, **6**, 197–212.
- Brandsdottir, B., W. Menke, P. Einarsson, R. S. White, and R. K. Staples (1997), Fåroe-Iceland Ridge experiment: 2. Crustal structure of the Krafla central volcano, *J. Geophys. Res.*, **102**, 7867–7886.
- Burov, E. B., and L. Guillou-Frottier (1999), Thermomechanical behavior of large ash flow calderas, *J. Geophys. Res.*, **104**, 23,081–23,109.
- Canales, J. P., J. A. Collins, J. Escartin, and R. S. Detrick (2000), Seismic structure across the rift valley of the Mid-Atlantic Ridge at $23^\circ 20'\text{N}$: Implications for crustal accretion processes at slow spreading ridges, *J. Geophys. Res.*, **105**, 28,411–28,425.
- Chevallier, L., and W. J. Verwoerd (1990), Influence of temperature on the distribution of stress and displacement in a volcano: A numerical approach, *Bull. Volcanol.*, **52**, 413–425.
- Cole, J. W., D. M. Milner, and K. D. Spinks (2005), Calderas and caldera structures: A review, *Earth Sci. Rev.*, **69**, 1–26.
- Courtillot, V. (1982), Propagating rifts and continental break-up, *Tectonics*, **1**, 239–250.
- Courtillot, V., A. Galdeano, and J.-L. Le Mouél (1980), Propagation of an accreting plate boundary: A discussion of new aeromagnetic data in the Gulf of Tadjurah and southern Afar, *Earth Planet. Sci. Lett.*, **47**, 144–160.
- Courtillot, V., R. Armijo, and P. Tapponnier (1987), Kinematics of the Sinaumli: Triple Junction and a two-phase model of Arabia-Africa rifting, in *Continental Extensional Tectonics*, edited by M. P. Coward, J. F. Dewey, and P. L. Hancock, *Geol. Soc. Spec. Publ.*, **28**, 559–573.
- Cowie, P. A., C. H. Scholtz, M. Edwards, and A. Malinverno (1993), Fault strain and seismic coupling on mid-ocean ridges, *J. Geophys. Res.*, **98**, 17,911–17,920.
- Crawford, W. C., S. C. Webb, and J. A. Hildebrand (1999), Constraints on melt in the lower crust and Moho at the East Pacific Rise, $9^\circ 48'\text{N}$, using seafloor compliance measurements, *J. Geophys. Res.*, **104**, 2923–2939.
- Dawson, P., B. Chouet, P. Okubo, A. Villaseñor, and H. Benz (1999), Three-dimensional velocity structure of the Kilauea caldera, Hawaii, *Geophys. Res. Lett.*, **26**, 2805–2808.
- De Chabaliér, J.-B., and J.-P. Avouac (1994), Kinematics of the Asal Rift (Djibouti) determined from the deformation of Fieale Volcano, *Science*, **265**, 1677–1681.
- Demange, J., and P. Puvilland (1990), *Champ géothermique d'Asal, Djibouti, synthèse des données*, Bur. de Rech. Geol. et Min., Orléans, France.
- Demange, J., L. Stieltjes, and J. Varet (1980), L'éruption d'Asal de Novembre 1978, *Bull. Soc. Geol. Fr.*, **7**, 837–843.
- De Natale, G., A. Zollo, A. Ferraro, and J. Virieux (1995), Accurate fault mechanism determinations for a 1984 earthquake swarm at Campi Flegrei caldera (Italy) during an unrest episode: Implications for volcanological research, *J. Geophys. Res.*, **100**, 24,167–24,185.
- Dobre, C., and L. Geoffroy (2003), Rift-zone development around a plume-related magma centre on the Isle of Skye (Scotland): A model for stress inversions, *Terra Nova*, **15**, 230–237.
- Dobre, C., and G. Peltzer (2007), Fluid-controlled faulting process in the Asal rift, Djibouti, from 8 yr of radar interferometry observations, *Geology*, **35**(1), 69–72, doi:10.1130/G23022A.1.
- Dobre, C., G. Peltzer, I. Manighetti, and E. Jacques (2005), Eight years of surface deformation in the Asal-Ghoubbet Rift (Afar Depression) observed with SAR data, *Eos Trans. AGU*, **86**(52), Fall Meet. Suppl., Abstract G42A-04.
- Dobre, C., I. Manighetti, L. Dorbath, C. Dorbath, D. Bertil, and J. C. Delmond (2007), Crustal structure and magmato-tectonic processes in an active rift (Asal-Ghoubbet, Afar, East Africa): 2. Insights from the

- 23-year recording of seismicity since the last rifting event, *J. Geophys. Res.*, doi:10.1029/2006JB004333, in press.
- Eberhart-Phillips, D. (1986), Three-dimensional velocity structure in the northern California coast ranges from inversion of local earthquake arrival times, *Bull. Seismol. Soc. Am.*, **76**, 1025–1052.
- Eberhart-Phillips, D. (1990), Three-dimensional *P* and *S* velocity structure in the Coalinga region, California, *J. Geophys. Res.*, **95**, 15,343–15,363.
- Ebinger, C., and M. Casey (2001), Continental break-up in magmatic provinces: An Ethiopian example, *Geology*, **29**, 527–530.
- Einarsson, P. (1991), Earthquakes and present-day tectonism in Iceland, *Tectonophysics*, **189**, 261–279.
- Ekström, G. (1994), Anomalous earthquakes on volcano ring-fault structures, *Earth Planet. Sci. Lett.*, **128**, 707–712.
- Escartin, J., P. A. Cowie, R. C. Searle, S. Allerton, N. C. Mitchell, C. J. MacLeod, and A. P. Slootweg (1999), Quantifying tectonic strain and magmatic accretion at a slow spreading ridge segment, Mid-Atlantic Ridge, 29°N, *J. Geophys. Res.*, **104**, 10,421–10,437.
- Evans, J. R., D. Eberhart-Phillips, and C. H. Thurber (1994), User's manual for simulp12 for imaging *Vp* and *Vp/Vs*: A derivative of the "Thurber" tomographic inversion simul3 for local earthquakes and explosions, *U.S. Geol. Surv. Open File Rep.*, 94-431.
- Feuillet, N., C. Nostro, C. Chiarabba, and M. Cocco (2004), Coupling between earthquake swarms and volcanic unrest at the Alban Hills Volcano (central Italy) modeled through elastic stress transfer, *J. Geophys. Res.*, **109**, B02308, doi:10.1029/2003JB002419.
- Feuillet, N., M. Cocco, C. Musumeci, and C. Nostro (2006), Stress interaction between seismic and volcanic activity at Mt Etna, *Geophys. J. Int.*, **164**, 697–718.
- Folch, A., and J. Martí (2004), Geometrical and mechanical constraints on the formation of ring-fault calderas, *Earth Planet. Sci. Lett.*, **221**, 215–225.
- Forslund, T., and A. Gudmundsson (1991), Crustal spreading due to dikes and faults in southwest Iceland, *J. Struct. Geol.*, **13**, 443–457.
- Foulger, G. R. (1988a), The Hengill triple junction, SW Iceland: 1. Tectonic structure and the spatial and temporal distribution of local earthquakes, *J. Geophys. Res.*, **93**, 13,507–13,523.
- Foulger, G. R. (1988b), The Hengill triple junction, SW Iceland: 2. Anomalous focal mechanisms and implications for processes within geothermal reservoir and at accretionary plate boundaries, *J. Geophys. Res.*, **93**, 13,507–13,523.
- Foulger, G. R., and R. E. Long (1984), Anomalous focal mechanisms: Tensile crack formation on an accreting plate boundary, *Nature*, **310**, 43–45.
- Foulger, G. R., R. E. Long, P. Einarsson, and A. Björnsson (1989), Implosive earthquakes at the accretionary plate boundary in northern Iceland, *Nature*, **337**, 640–642.
- Foulger, G. R., B. R. Julian, D. P. Hill, A. M. Pitt, P. E. Malin, and E. Shalev (2004), Non-double-couple microearthquakes at Long Valley caldera, California, provide evidence for hydraulic fracturing, *J. Volcanol. Geotherm. Res.*, **132**, 45–71.
- Frohlich, C. (1984), Earthquakes with non double couple mechanisms, *Science*, **264**, 804–809.
- Gerla, P. J. (1988), Stress and fracture evolution in a cooling pluton: An example from the Diamond Joe Stock, western Arizona, U.S.A., *J. Volcanol. Geotherm. Res.*, **34**, 267–282.
- Gray, J. P., and J. J. Monaghan (2004), Numerical modeling of stress fields and fracture around magma chambers, *J. Volcanol. Geotherm. Res.*, **135**, 259–283.
- Gudmundsson, A. (1998), Magma chambers modeled as cavities explain the formation of rift zone central volcanoes and their eruption and intrusion statistics, *J. Geophys. Res.*, **103**, 7,401–7,412.
- Gudmundsson, O., B. Brandsdóttir, W. Menke, and G. E. Sigvaldason (1994), The crustal magma chamber of the Katla volcano in south Iceland revealed by 2-D seismic undershooting, *Geophys. J. Int.*, **119**, 277–296.
- Hayward, N. J., and C. J. Ebinger (1996), Variations in the long-axis segmentation of the Afar rift system, *Tectonics*, **15**, 244–257.
- Hirth, G., J. Escartin, and J. Lin (1998), The rheology of the lower oceanic crust: implications for lithospheric deformation at mid-ocean ridges, in *Faulting and Magmatism at Mid-Ocean Ridges*, *Geophys. Monogr. Ser.*, vol. 106, edited by R. W. Buck et al., pp. 291–303, AGU, Washington, D. C.
- Hussenoeder, S. A., G. M. Kent, and R. S. Detrick (2002), Upper crustal seismic structure of the slow spreading Mid-Atlantic Ridge, 35°N: Constraints on volcanic emplacement processes, *J. Geophys. Res.*, **107**(B8), 2156, doi:10.1029/2001JB001691.
- Julian, B. R. (1983), Evidence of dyke intrusion earthquake mechanism near Long Valley caldera, California, *Nature*, **303**, 681–685.
- Julian, B. R., A. D. Miller, and G. R. Foulger (1988), Nondouble-couple earthquakes: 1. Theory, *Rev. Geophys.*, **36**, 525–549.
- Kanamori, H., and D. L. Anderson (1975), Theoretical basis of some empirical relations in seismology, *Bull. Seismol. Soc. Am.*, **65**, 1073–1095.
- Klein, F. W. (1978), Hypocenter location program HYPOINVERSE, Part 1, Users guide to versions 1, 2, 3 and 4, *U.S. Geol. Surv. Open File Rep.*, 78-694.
- Kong, L. S., S. C. Solomon, and G. M. Purdy (1992), Microearthquake characteristics of a mid-oceanic ridge along-axis high, *J. Geophys. Res.*, **97**, 1659–1685.
- Lagabriele, Y., E. Garel, O. Dauteuil, and M. H. Cormier (2001), Extensional faulting and caldera collapse in the axial region of fast spreading ridges: Analog modeling, *J. Geophys. Res.*, **106**, 2005–2015.
- Le Dain, A.-Y., B. Robineau, and P. Tapponnier (1979), Les effets tectoniques de l'événement sismique et magmatique de Novembre 1978 dans le rift d'Asal-Ghoubbet, *Bull. Soc. Geol. Fr.*, **7**, 817–822.
- Lépine, J.-C., and A. Hirn (1992), Seismotectonics in the Republic of Djibouti linking the Afar Depression and the Gulf of Aden, *Tectonophysics*, **209**, 65–86.
- Lépine, J.-C., J.-C. Ruegg, and A. M. Anis (1980), Sismicité du rift d'Asal-Ghoubbet pendant la crise sismo-volcanique de Novembre 1978, *Bull. Soc. Geol. Fr.*, **7**, 809–816.
- Lipman, P. W. (1997), Subsidence of ash-flow calderas: Relation to caldera size and magma chamber geometry, *Bull. Volcanol.*, **59**, 198–218.
- Madge, L. S., A. H. Barclay, D. R. Toomey, R. S. Detrick, and J. A. Collins (2000), Crustal magma plumbing within a segment of the Mid-Atlantic Ridge, 35°N, *Earth Planet. Sci. Lett.*, **175**, 55–67.
- Manighetti, I. (1993), Dynamique des systèmes extensifs en Afar, thèse de Doctorat, 240 pp., Univ. de Pierre et Marie Curie, Paris.
- Manighetti, I., P. Tapponnier, V. Courtillot, S. Gruszow, and P.-Y. Gillot (1997), Propagation of rifting along the Arabia-Somalia plate boundary: The gulfs of Aden and Tadjoura, *J. Geophys. Res.*, **102**, 2681–2710.
- Manighetti, I., P. Tapponnier, P.-Y. Gillot, E. Jacques, V. Courtillot, R. Armijo, J.-C. Ruegg, and G. King (1998), Propagation of rifting along the Arabia-Somalia plate boundary: Into Afar, *J. Geophys. Res.*, **103**, 4947–4974.
- Manighetti, I., G. C. P. King, Y. Gaudemer, C. H. Scholtz, and C. Doubre (2001a), Slip accumulation and lateral propagation of active normal faults in Afar, *J. Geophys. Res.*, **106**, 13,667–13,696.
- Manighetti, I., P. Tapponnier, V. Courtillot, Y. Gallet, E. Jacques, and Y. Gillot (2001b), Strain transfer between disconnected, propagating rifts in Afar, *J. Geophys. Res.*, **106**, 13,613–13,665.
- Manighetti, I., G. King, and C. Sammis (2004), The role of the off-fault damage in the evolution of normal faults, *Earth Planet. Sci. Lett.*, **217**, 399–408.
- Manighetti, I., M. Campillo, C. Sammis, P. M. Mai, and G. King (2005), Evidence for self-similar, triangular slip distributions on earthquakes: Implications for earthquake and fault mechanics, *J. Geophys. Res.*, **110**, B05302, doi:10.1029/2004JB003174.
- Miller, D. S., and R. B. Smith (1999), *P* and *S* velocity structure of the Yellowstone volcanic field from local earthquake and controlled-source tomography, *J. Geophys. Res.*, **104**, 15,105–15,121.
- Mlynarski, M., and J. Zlotnicki (2001), Fluid circulation in the active emerged Asal Rift (East Africa, Djibouti) inferred from self-potential and Telluric-Telluric prospecting, *Tectonophysics*, **339**, 455–472.
- Mori, J., and C. McKee (1987), Outward-dipping ring-fault structure at Rabaul Caldera as shown by earthquake locations, *Science*, **235**, 193–195.
- Mori, J., R. White, D. Harlow, P. Okubo, J. Power, R. Hoblitt, E. Laguerre, L. Lanuza, and B. Bautista (1996), Volcanic earthquakes following the 1991 climactic eruption of Mount Pinatubo, Philippines: Strong seismicity during a waning eruption, in *Fire and Mud: Eruptions and Lahars of Mount Pinatubo, Philippines*, edited by C. G. Newhall and R. S. Punongbayan, pp. 339–350, Univ. of Wash. Press, Seattle.
- Needham, H. D., P. Choukroune, J.-L. Cheminée, X. Le Pichon, J. Francheteau, and P. Tapponnier (1976), The accreting plate boundary: Ardoukoba Rift and the oceanic rift valley, *Earth Planet. Sci. Lett.*, **28**, 439–453.
- Nettles, M., and G. Ekström (1998), Faulting mechanism of anomalous earthquakes near Bardarbunga, Iceland, *J. Geophys. Res.*, **103**, 17,973–17,983.
- Nicolas, A., C. Freydisier, M. Godard, and A. Vauchez (1993), Magma chambers at oceanic ridges: How large?, *Geology*, **21**, 53–56.
- Parson, L. M., et al. (1993), En echelon axial volcanic ridges at the Reykjanes Ridge: A life cycle of volcanisms and tectonics, *Earth Planet. Sci. Lett.*, **117**, 73–87.
- Pechmann, J. C., J. C. Bernier, S. J. Nava, F. M. Terra, and W. Arabasz (2001), Correction of systematic time-dependant coda magnitude errors in the Utah and Yellowstone National Park region earthquake catalog, 1981–2001, *Eos Trans. AGU*, **82**(47), Fall Meet. Suppl., Abstract S11B-0572.

- Pollard, D., P. Delaney, W. Duffield, E. Endo, and A. Okamura (1983), Surface deformation in volcanic rift zones, *Tectonophysics*, **94**, 541–584.
- Prejean, S., A. Stork, W. Ellsworth, D. Hill, and B. Julian (2003), High precision earthquake locations reveal seismogenic structure beneath Mammoth Mountain, California, *Geophys. Res. Lett.*, **30**(24), 2247, doi:10.1029/2003GL018334.
- Roche, O., T. H. Druitt, and O. Merle (2000), Experimental study of caldera formation, *J. Geophys. Res.*, **105**, 395–416.
- Rubin, A. (1990), A comparison of rift zone tectonics in Iceland and Hawaii, *Bull. Volcanol.*, **52**, 302–319.
- Ruegg, J.-C. (1975), Structure profonde de la croûte et du manteau supérieur du Sud-Est de l'Afar d'après les données sismiques, *Ann. Geophys.*, **31**, 329–360.
- Ruegg, J.-C., and M. Kasser (1987), Deformation across the Asal-Ghoubbet Rift, Djibouti, uplift and crustal extension, 1979–1986, *Geophys. Res. Lett.*, **14**, 745–748.
- Ruegg, J.-C., J.-C. Lépine, and A. Tarantola (1979), Geodetic measurements of rifting associated with a seismo-volcanic crisis in Afar, *Geophys. Res. Lett.*, **6**, 817–820.
- Ruegg, J.-C., F. Gasse, and P. Briole (1990), Mouvements du sol holocènes dans le rift d'Asal à Djibouti, *C. R. Acad. Sci.*, **310**, 1687–1694.
- Shimizu, H., S. Ueki, and J. Koyama (1987), A tensile-shear crack model for the mechanism of volcanic earthquakes, *Tectonophysics*, **144**, 287–300.
- Sohn, R. A., A. H. Barclay, and S. C. Webb (2004), Microearthquake patterns following the 1998 eruption of Axial Volcano, Juan de Fuca Ridge: Mechanical relaxation and thermal strain, *J. Geophys. Res.*, **109**, B01101, doi:10.1029/2003JB002499.
- Stein, R., P. Briole, J.-C. Ruegg, P. Tapponnier, and F. Gasse (1991), Contemporary, Holocene, and Quaternary deformation of the Asal Rift, Djibouti: Implications for the mechanics of slow spreading ridges, *J. Geophys. Res.*, **96**, 21,789–21,806.
- Stieljes, L. (1980), Carte géologique du rift d'Asal, République de Djibouti (Dépression Afar, Est africain), Centre Natl. de la Res. Sci., Paris.
- Tait, S., C. Jaupart, and S. Vergnolle (1989), Pressure, gas content and eruption periodicity of a shallow, crystallizing magma chamber, *Earth Planet. Sci. Lett.*, **92**, 107–123.
- Tapponnier, P., R. Armijo, I. Manighetti, and V. Courtillot (1990), Book-shelf faulting and horizontal block rotations between overlapping rift zones in southern Afar, *Geophys. Res. Lett.*, **17**, 1–4.
- Tarantola, A., J.-C. Ruegg, and J.-C. Lépine (1979), Geodetic evidence for rifting in Afar: A brittle-elastic model of the behaviour of the lithosphere, *Earth Planet. Sci. Lett.*, **45**, 435–444.
- Tarantola, A., J.-C. Ruegg, and J.-P. Lépine (1980), Geodetic evidence for rifting in Afar, 2. Vertical displacements, *Earth Planet. Sci. Lett.*, **48**, 363–370.
- Thurber, C. H. (1983), Earthquake locations and three-dimensional crustal structure in the Coyote Lake area, central California, *J. Geophys. Res.*, **88**, 8226–8236.
- Thurber, C. H. (1984), Seismic detection of the summit of magma complex of Kilauea volcano, Hawaii, *Science*, **223**, 165–167.
- Tilling, R. I., and J. J. Dvorak (1993), Anatomy of a basaltic volcano, *Nature*, **363**, 125–133.
- Tolstoy, M., D. R. Bohnenstiehl, M. H. Edwards, and G. J. Kurras (2001), Seismic character of volcanic activity at the ultraslow-spreading Gakkel ridge, *Geology*, **29**, 1139–1142.
- Toomey, D. R., and G. R. Foulger (1989), Tomographic inversion of local earthquake data from the Hengill-Grensdalur central volcano complex, Iceland, *J. Geophys. Res.*, **94**, 17,497–17,510.
- Toomey, D. R., G. M. Purdy, S. C. Solomon, and W. S. D. Wilcock (1990), The Three-Dimensional seismic velocity structure of the East Pacific Ridge near latitude 9°30'N, *Nature*, **347**, 639–645.
- Troise, C., G. De Natale, F. Pingue, and A. Zollo (1997), A model for earthquake generation during unrest episodes at Campi Flegrei and Rabaul calderas, *Geophys. Res. Lett.*, **24**, 1575–1578.
- Troise, C., F. Pingue, and G. De Natale (2003), Coulomb stress changes at calderas: Modeling the seismicity of Campi Flegrei (southern Italy), *J. Geophys. Res.*, **108**(B6), 2292, doi:10.1029/2002JB002006.
- Tryggvason, E. (1986), Multiple magma reservoirs in a rift zone volcano: Ground deformation and magma transport during the September 1984 eruption of Krafla, Iceland, *J. Volcanol. Geotherm. Res.*, **28**, 1–44.
- Van Ngoc, P., D. Boyer, J.-L. Le Mouél, and V. Courtillot (1981), Identification of a magma chamber in the Ghoubbet-Asal Rift (Djibouti) from a magnetotelluric experiment, *Earth Planet. Sci. Lett.*, **52**, 372–380.
- Varet, J. (1978), Geology of central and southern Afar (Ethiopia and Djibouti Republic), 124 p., Centre Natl. de la Res. Sci., Paris.
- Vigny, C., J.-B. de Chabalière, J.-C. Ruegg, P. Huchon, K. L. Feigl, R. Cattin, L. Asfaw, and K. Kanbari (2007), Twenty-five years of geodetic measurements along the Tadjoura-Asal rift system, Djibouti, East Africa, *J. Geophys. Res.*, doi:10.1029/2004JB003230, in press.
- Wilcock, W. S. D., S. C. Solomon, G. M. Purdy, and D. R. Toomey (1995), Seismic attenuation structure of the East Pacific Rise near 9°30'N, *J. Geophys. Res.*, **100**, 24,147–24,165.
- Wolfe, C. J., G. M. Purdy, D. R. Toomey, and S. Solomon (1995), Micro-earthquake characteristics and crustal velocity structure at 29°N on the Mid-Atlantic Ridge: The architecture of a slow spreading segment, *J. Geophys. Res.*, **100**, 24,449–24,472.

J. C. Delmond, Volcanologic Observatories, IPGP, 4 Place Jussieu, F-75252 Paris, France.

C. Dorbath and L. Dorbath, EOST, 5, rue René Descartes, F-67084 Strasbourg, France.

C. Doubre, Department of Earth and Space Sciences, Geology Building, 595 Charles E. Young Drive East, University of California, Los Angeles, CA 90095-1567, USA.

E. Jacques, Laboratoire de Tectonique, IPGP, 4 Place Jussieu, F-75252 Paris, France.

I. Manighetti, Laboratoire de Géophysique Interne et Tectonophysique, BP 53, F-38041 Grenoble Cedex 9, France.